UNAFLOW: a holistic wind-tunnel experiment about the aerodynamics aerodynamic response of floating wind turbines under imposed surge motion

Alessandro Fontanella[1], Ilmas Bayati[2], Robert Mikkelsen[3], Marco Belloli[1], and Alberto Zasso[1]

[1]Mechanical Engineering Department, Politecnico di Milano, Milano, Via La Masa 1, 20156, Italy.
[2]Maritime Research Institute Netherlands (MARIN), Wageningen, 6708 PM, The Netherlands.
[3]Technical University of Denmark (DTU), Department of Wind Energy, Lyngby, Denmark.

Correspondence: Alessandro Fontanella (alessandro.fontanella@polimi.it)

Abstract. Floating offshore wind turbines are subjected to large motions ~~because of~~ due to the additional degrees of freedom ~~offered by~~ of the floating foundation. The rotor ~~operates in highly dynamic~~ often operates in highly-dynamic inflow conditions and this ~~is deemed to have~~ has a significant effect on the ~~aerodynamic loads, as well as on the wind~~ overall aerodynamic response and turbine wake. ~~Floating wind turbines and floating farms are designed by means of numerical tools, that have to model these unsteady aerodynamic phenomena to be predictive of reality.~~ Experiments are needed to get a deeper understanding of ~~the~~ unsteady aerodynamics, and hence ~~leverage~~ exploit this knowledge to develop better models, ~~as well as~~ and to produce data for the validation and calibration of the existing numerical tools. This paper presents a wind-tunnel ~~scale-model~~ experiment about the unsteady aerodynamics of floating ~~wind turbines that followed a radically different approach than the other existing experiments. The experiment covered any aspect of the problem in a coherent and structured manner, that allowed to produce a low-uncertainty data for the validation of numerical model. The data covers the unsteady aerodynamics of the floating wind turbine in terms of~~ turbines subjected to surge motion. The experiment results cover blade forces, ~~rotor~~ rotor-integral forces and wake. 2D sectional model tests were carried ~~to study the aerodynamics~~ out to characterize the aerodynamic coefficients of a low-Reynolds ~~blade profile subjected to a~~ airfoil subjected to harmonic variation of the angle of attack. The lift coefficient shows ~~an~~ a hysteresis cycle that extends in the linear region and grows in strength for higher ~~motion frequencies. The knowledge gained in 2D sectional model tests was exploited to design the rotor of a 1/75 scale model of the DTU 10MW that was used to perform imposed surge motion tests in a wind tunnel. The tower-top forces were measured for several combinations of mean wind speed, surge amplitude and frequency to assess the effect of unsteady aerodynamics on the~~ pitching frequencies. Knowledge about the airfoil aerodynamic response was utilized to define the wind and surge-motion conditions of the full-turbine experiment. The global aerodynamic response of the ~~system. The thrust force , that plays a crucial role in~~ wind turbine is evaluated from rotor-thrust force measurements, because thrust-force drives the along-wind dynamics ~~of a floating wind turbinemostly follows the~~ in any floating turbine. Experimental data follow reasonably well predictions of quasi-steady theory ~~.~~ for reduced frequency up to 0.5. For higher surge-motion frequencies, unsteady effects may be present. The near-wake of the wind turbine was ~~studied~~ investigated by means of hot-wire measurements~~, and PIV was utilized to visualize the tip vortex. It is seen that~~ . The wake energy is increased at the surge-motion frequency, and the increment is proportional to the

maximum surge velocity. A spatial analysis shows the wake energy ~~is increased~~ increment is in correspondence of ~~the motion frequency and this is likely to be associated with~~ blade-tip and of the most loaded rotor region. PIV was utilized to visualize the blade-tip vortex ~~, which~~ and it is found the vortex travel speed is modified in presence of surge motion.

1 Introduction

Floating offshore wind is receiving ~~a~~ growing interest as it ~~makes it possible to harvest the~~ enables deep sea wind energy resource ~~of deep waters, which cannot be exploited a cost competitive price~~to be harvested at a competitive price, which is not possible with conventional bottom-fixed ~~wind turbines~~solutions. Floating offshore wind turbines (FOWTs) are subjected to large and low-frequency motions that ~~are the cause of~~ cause unsteady aerodynamics effects. The rotor of an FOWT operates in dynamic inflow conditions ~~de Vaal et al. (2014), mainly for two reasons: the~~ and, as pointed out by de Vaal et al. (2014), this occurs for two main reasons: platform motion modifies the wind speed seen by the rotor ~~, and~~ and in some cases moves the rotor in its own wake. This has a significant effect on the aerodynamic loads and, consequently, on the ~~response of the FOWT~~ FOWT response. Moreover, ~~the~~ platform motions result ~~into~~ in large-scale motions of the wind turbine wake, which are relevant for the wake-interaction in floating farms ~~Wise and Bachynski (2020)~~(Wise and Bachynski (2020)).

Wind turbines and wind farms are ~~designed and studied~~ often designed by means of ~~numerical simulation tools~~ engineering tools that were adapted from land-based tools. In this adaptation process, aerodynamic models have remained almost unchanged. However, floating turbines are subjected to peculiar inflow conditions that are not present in land-based turbines. The rotor of land-based turbines undergoes small-amplitude motions associated to the tower flexible response. The motion of an FOWT rotor is in large part set by the rigid-body motion of the support platform and is in general of higher amplitude and lower frequency than in land-based turbines. The accuracy of land-based-derived aerodynamic tools in this new inflow conditions is yet to be assessed. An accurate prediction of the aerodynamic response caused by rotor motion is crucial. As mentioned, this occurs at lower frequencies than in land-based turbines and, unlike the latter, causes significant interactions with the turbine controller (i.e., the aerodynamic response in FOWTs is inside the bandwidth of the turbine controller) that may lead to instability. Experiments play a crucial role in verifying whether the aerodynamic codes are accurate also for floating turbines, ~~that are in large part developed for bottom-fixed wind turbines. Experiments are needed to assess wether these models are predictive also for wind turbines with a floating foundation,~~ to get a deeper understanding of the peculiar aerodynamic phenomena that occurs when the wind turbine undergoes large motions and, based on this knowledge, to develop better simulations tools. ~~Even though the importance of the aerodynamics of FOWTs is widely recognized, few are the experiments that tried to~~

To date, there are few wind-tunnel experiments that shed light into ~~this topic.~~ the unsteady aerodynamic response of floating turbines. ~~In Farrugia et al. (2014)~~ Farrugia et al. (2014) carried out a wave-basin ~~tests were carried out about a TLP-FOWT subjected to regular waves, measuring~~ test campaign to measure the wind turbine power and wake for a TLP-FOWT subjected to regular waves. ~~In Hu et al. (2015) ,~~ Hu et al. (2015) utilized a 1/300 Froude-scaled wind turbine model ~~was installed on~~ and a 3-DOF motion simulator in a ~~wind tunnel. PIV was used to obtain a flow description in the near wake region~~ wind-tunnel to assess the influence of surge motion on structural loads, and its effect on the near wake ($x/D<2$~~) and structural loads where~~

measured when the system was subjected to surge motion. In Fu et al. (2019) , wind tunnel experiments were performed to assess , PIV measurements). Fu et al. (2019) performed a set of wind tunnel tests to quantify the effect of pitch and roll oscillations on power output and wake of a wind turbine scale model (12cm rotor diameter). The experiment did not consider the rotor thrust force, that is strongly coupled with the platform motions. . Rotor thrust was not measured. In Schliffke et al. (2020) Schliffke et al. (2020) studied the wake (at a distance of 4.6D) of a porous disk model is used to represent a 2MW FOWT at 1/500 scale , and study its wake at a distance of 4.6D when subjected to an with a porous disk model subjected to imposed surge motion. The porous disk concept A porous disk model has some inherent limitations: it is not valid to study the near wake and does not reproduce the local aerodynamic loads of the blades. In the wind tunnel tests of Bayati et al. (2016) a high-fidelity 1/75 scale model of the DTU 10MW wind turbine is used to study the One goal of the EU H2020 LIFES50+ project was to develop a reliable aerodynamic model of an FOWT rotor to be used in hybrid wave-basin experiments (a numerical rotor is coupled to a physical scale-model of the floating platform, as done by Sauder et al. (2016)). To this purpose, Bayati et al. (2016) investigated the effect of imposed surge and pitch motion on the rotor thrust force. Measurements are compared to FAST simulations to rotor-thrust with a 1/75 scale-model of the DTU 10MW. Measurements were utilized to assess the prediction capabilities of AeroDyn (Moriarty and Hansen (2005)) with respect to FOWTs. Numerical and experimental results showed some discrepancies that suggested the need to study the problem further. In Bayati et al. (2017c) , a second test campaign is carried out to study by means The analysis evidenced some differences between simulation and experiment that suggested a further study of the problem. Bayati et al. (2017c) carried out a second wind-tunnel test campaign with focus on the effect of surge motion of the wind turbine wake, that was measured with hot-wire measurements the near-wake of the same scale model under imposed surge motion. probes.

In parallel with wind-tunnel experiments, a series of floating turbine model-tests was performed in different wave-basins. Among the goals of these experiment was to investigate the effect of turbine aerodynamic loads on the global response of the system. Goupee et al. (2012) investigated at 1/50 scale the response of three 5MW FOWTs to wind and wave excitation. The blades of the turbine model were a geometrically scaled version of the NREL 5MW blade, and the aerodynamic performance (thrust and power) of the rotor was not representative of the full-scale turbine. This was found to be a consequence of the Froude-scaled low-Reynolds wind. To cope with this issue, Goupee et al. (2014) designed a new rotor to carry out a second set of tests. This second campaign proved that wind-turbine aerodynamic loads must be reproduced correctly when assessing the global response of FOWTs in wave-basin tests. More recent research efforts, like the work of Goupee et al. (2017) or of Bredmose et al. (2017), studied the interaction between turbine-control, aerodynamic forces, and platform motions. Overall, integrated wave-basin tests proved to be very useful in studying the coupled response of floating turbines modeling simultaneously wave excitation, wind, and turbine control. However, reproducing the turbine aerodynamic response is hindered by the low-Reynolds number imposed by Froude-scaling (Bayati et al. (2018)) and by quality of the wind environment (Martin et al. (2014)). With these limitations, reproducing a realistic turbine wake is usually out of reach.

The UNAFLOW experiment unsteady response of FOWTs is still an open question. In this respect, this article presents the wind-tunnel scale-model experiment that was carried out as part of the IRPWind UNAFLOW project. The goal of the experiment was built on the experience gained in Bayati et al. (2016, 2017c). The aim of the project was to study the unsteady

~~aerodynamics of FOWTs following a holistic and systematic approach. The experiment generated a comprehensive database, that covers the unsteady aerodynamics of the wind turbine blade, the rotor forces and the near wake.~~ aerodynamic response and wake for an FOWT subjected to large surge (i.e., translational) motion, as it normally occurs in operation. Studying these issues at small scale has some limitations because it is not possible to exactly reproduce all the physics of a full-scale system (e.g., structural response, inflow conditions). However, this disadvantage is offset by the possibility to accurately control and better know the test conditions, and to implement more measurements than in a real turbine. The main contributions of this work are as follows:

- a preliminary 2D experiment is performed to characterize the airfoil used for the scaled turbine blades. Unlike in previous studies, knowledge of the unsteady aerodynamic response of the blade airfoil is leveraged to select the wind and surge-motion conditions for the full-turbine experiment. In addition, 2D data are a reliable polar-dataset that can be used to create numerical models of the experiment;
- accuracy of force measurements is improved with respect to the previous test campaigns of Bayati et al. (2016) and Bayati et al. (2017c). The flexible tower in LIFES50+ tests created issues in the measurements, making their use difficult for code validation;
- thrust force measurements from full-turbine experiments are compared to predictions of a quasi-steady rotor-disk model. This model is often relied on when building reduced-order FOWT models for control applications (e.g., Lemmer et al. (2020); Fontan), and assessing its prediction capabilities is therefore crucial for developing effective controllers. It is found the thrust force follows the quasi-steady theory for reduced frequency below 0.5;
- the wind turbine wake is measured with hot-wire probes to describe and quantify the effect of surge-motion on its energy content. PIV measurements are utilized to assess the influence of surge-motion on the position of tip-vortex inside the wake. The wake energy is increased in correspondence of the motion frequency.

The impact this paper and the UNAFLOW experiment have on research about FOWT unsteady aerodynamics is:

- additional knowledge about the unsteady aerodynamics of an FOWT. In particular, the analysis is carried out with a system engineering vision of the problem, that considers the response of the entire floating system. Its findings may have an impact on blade design, wind turbine control, wake interaction and wind farm control;
- experimental methodology. The UNAFLOW experiment is the result of a joint effort of different research groups, some expert in numerical simulations and some in wind-tunnel experiments. The experiment followed an integrated approach: results of numerical computations and 2D experiments were utilized to design full-turbine experiments, which results were in turn used for validation of numerical tools. Because of these aspects, the experiment can be considered ~~as~~ among the most advanced ~~wind tunnel test on the topic of unsteady FOWT~~ wind-tunnel tests about FOWT unsteady aerodynamics to date;

– database. Differently than the previous test campaigns of Bayati et al. (2016) and Bayati et al. (2017c), the UNAFLOW experiment generated a comprehensive database that covers in a coherent manner aerodynamic coefficients of the blade airfoil, rotor-integral forces and near-wake. ~~Thanks to the systematic approach, the experimental data are featured by a low uncertainty level, that promotes their use as a benchmark for the development of~~ The database is accessible at:

https://doi.org/10.5281/zenodo.4740005

The systematic approach of the experiment makes data especially useful for validating numerical tools. ~~In Cormier et al. (2018), measurements were compared to~~ Cormier et al. (2018) utilized the UNAFLOW data to assess predictions of a BEM, a free-vortex and a fully-resolved CFD model. A second comparison ~~withnumerical models~~ with numerical tools was recently carried out ~~in Mancini et al. (2020)concerning the rotor thrust and power. The full dataset of the UNAFLOW experiments is freely available for the community for further studies.~~ by Mancini et al. (2020). The UNAFLOW dataset is currently used for the validation of numerical codes in the IEA Wind Task 30 OC6 project.

~~The aim of this paper is to twofold. First it presents the experiment, the methodology it was followed to design it, and that was used to carry out measurements later. Second, it presents the available dataset, serving as an accompaniment to them, and summarizes the most significant results from the experiment.~~ The structure of the remainder of ~~the~~ this paper is as follows. Section 2 describes the approach ~~that was~~ followed to design the experiment, and to select the ~~tested~~ wind and surge-motion conditions. Section 3 presents the 2D sectional model tests that were carried out at the Technical University of Denmark (DTU) Red wind tunnel, to characterize the aerodynamic coefficients of the SD7032 airfoil, used in the ~~scale model turbine~~ turbine model blades. Section 4 describes the full-turbine experiment, with emphasis on the wind turbine scale model and ~~the~~ measurements that were carried out. Section 5 reports the main findings of the full-turbine experiments with ~~surge motion~~surge-motion, in particular those about ~~the rotor thrust~~ rotor-thrust force, the energy content of the near-wake, and the tip-vortex~~structure~~. Section 6 draws the conclusions and gives some recommendations for future research.

2 Concept and design of the experiment

~~The rotor of an FOWT is often working in strong unsteady conditions, because of the~~ FOWTs undergo large rigid-body motions that ~~arise because the low-compliance~~ are due to the high-compliance of the floating ~~platform and~~ foundation and wind/wave excitation. ~~The UNAFLOW projects~~ Consequently, the rotor of an FOWT often operates in strong unsteady-flow conditions The UNAFLOW project studied the unsteady behavior of an FOWT rotor, ~~and~~ with the core of the experimental activity ~~was~~ towards an extensive wind tunnel test campaign with a high-fidelity wind turbine scale model subjected to imposed surge motion. The wind turbine was a 1/75 model of the DTU 10MW ~~Bak et al. (2013)~~(Bak et al. (2013)), with a 2.38m diameter rotor designed primarily to match the thrust and secondarily the power coefficient of the reference wind turbine. The purpose of the wind tunnel experiment was ~~tp~~ to provide a large dataset of rotor integral loads and wake measurements for several wind-turbine operating and motion conditions, selected to be realistic for a multi-megawatt FOWT. 2D sectional airfoil experiments

were carried out prior to the full-turbine tests, to guide the selection of the motion conditions for the turbine scale model, and to support the creation of numerical models of the experiment.

2.1 Wind conditions

The experiment considered three operating conditions which are reported in ~~table~~ Tab. 1. No closed-loop control strategy is utilized, ~~and the~~ rotor speed and ~~the collective pitch angles~~ collective pitch angle were fixed. ~~In the first two conditions~~At RATED1 and RATED2, the wind turbine is operated at the optimum full-scale value of tip-speed ratio (TSR) and power is extracted with maximum efficiency (i.e., the maximum power coefficient is achieved). ~~Being the TSR~~ Since TSR is the same, the angle of attack (AoA) along the blade is ~~the same~~ equal in the RATED1 and RATED2 conditions. In the ~~second condition ,~~ above-rated condition (ABOVE) the TSR is lower and the collective pitch angle is ~~increase, to get a lower powercoefficient~~increased, to preserve rated power. Experiments were carried out in smooth flow conditions, and the turbulence ~~index~~ intesity across the test section height was approximately 2%.

Table 1. Tested wind turbine operating conditions (V is the average wind speed, RS is the rotor speed, CP is the rotor collective pitch angle).

Condition	V [m/s]	RS [rpm]	TSR [-]	CP [deg]
RATED1	2.5	150	7.5	0
RATED2	4.0	241	7.5	0
ABOVE	6.0	265	5.5	12.5

Figure 1 shows the Reynolds number along the span of the ~~wind-turbine scale-model~~ turbine-model blade in the three operating conditions of ~~Table~~ Tab. 1. The Reynolds number is over 80k for most of the blade span in RATED2 and ABOVE conditions, and it drops to 50k in RATED1 wind speed. 2D airfoil sectional model experiments were carried out to measure the aerodynamic coefficients of the blade airfoil for a range of Reynolds number close to those ~~experience by the blade in~~ experienced by the full-turbine ~~tests~~blade.

2.2 Motion conditions

The aim of the experiment was to investigate the unsteady aerodynamics of an FOWT rotor ~~associated with~~ due to the rigid-body motion of the support platform. The unsteady aerodynamic problem is a complex multi-physics subject: ~~the~~ platform motion is driven by ~~the~~ wave excitation and depends on the characteristics of the platform itself. To keep the focus on the aerodynamic problem, some simplifying assumptions were made for what concerns ~~the~~ wave simulation and the resulting motion. The ~~wind turbine~~ wind-turbine model was forced to move in the surge direction and the other platform motions were not considered. The surge motion was selected because it produces an along-wind motion of the ~~wind turbine~~structure, which is in turn cause of ~~a large variation~~ large variations of the wind speed seen by the rotor. Moreover, in the surge motion, any

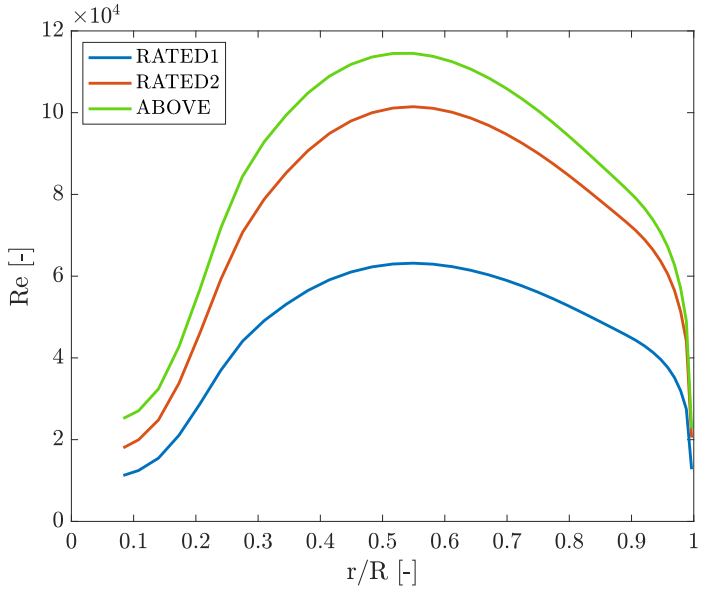

Figure 1. Reynolds number along the span (r/R is the non-dimensional radial position) of the ~~wind-turbine scale-model~~ turbine-model blade in the three operating conditions of the experiment.

point of the ~~wind turbine~~ rotor moves with the same velocity. This simplifies the modeling of the ~~aerodynamics~~ system as the effective wind speed is uniform across the rotor.

The surge motion x considered in the experiments is mono-harmonic:

$$x(t) = A_s \sin(2\pi f_s t)\,, \tag{1}$$

where A_s and f_s are the amplitude and frequency of motion respectively. The experiment investigated several mono-harmonic motions, obtained from the combination of different values of amplitude and frequency.

Seven frequencies were selected in the range [0.125 - 2] Hz (model scale) which corresponds to the low-frequency range for ~~semi-sub~~ semi-submersible and spar platforms. Large motions are expected in this range of frequencies, as ~~the~~ rigid-body motion modes are excited in resonance. The maximum frequency investigated in the full-turbine experiment was limited to 2 Hz to avoid exciting the first ~~tower~~ fore-aft ~~flexible mode.~~ (FA) mode. Resonant excitation of this mode occurs due to higher harmonics of the imposed surge-motion, which amplitude decreases with frequency. The frequency of the first FA mode for the turbine model of the previous LIFES50+ tests (Bayati et al. (2017c)) was 4.25 Hz, and the resonant response penalized force measurements. The UNAFLOW turbine adopted a stiffer tower with the first FA mode at 6.75 Hz (the scaled frequency of the DTU 10MW is 6.29 Hz) and this improved measurements accuracy. The effect the frequency of motion has on the rotor aerodynamics is qualitatively described by the unit-less wake reduced-velocity parameter introduced ~~in~~ by Bayati et al.

(2017a):

$$V_w^* = \frac{V}{f_s D}, \tag{2}$$

where ~~D is~~ the rotor diameter ~~, which~~ D is adopted as ~~reference length, since it is widely used to describe the wake interaction in wind turbines~~characteristic reference length. A high V_w^* means the air particles flow across the wind turbine in a short time, ~~its~~ their path is not influenced by the wind turbine motion and ~~the~~ flow is quasi-steady. The lower the wake reduced velocity, the higher the unsteady effects.

Four amplitudes were tested for each combination of frequency and mean wind speed V. ~~The selection of the values of amplitude~~ Selection of amplitude values was based on the maximum surge velocity:

$$\max(\dot{x})\max(\dot{x}(t)) = \Delta V = 2\pi f_s A_s\,. \tag{3}$$

The ~~surge motion~~ surge-motion causes a variation of the ~~angle of attack along the~~ AoA along blades that is, in first approximation, proportional to:

$$\Delta V^* = \frac{\Delta V}{V}\,. \tag{4}$$

The four amplitude values were initially selected to achieve, for any pairing of wind speed and motion frequency, $\Delta V^* = 1/20, 3/80, 1/40, 1/80$. At low frequencies, the desired amplitude of motion was ~~bigger~~ larger than the stroke of the hydraulic actuator and it was reduced ~~in reason of this constraint~~consequently. Moreover, the amplitudes of the 1 Hz-frequency cases were increased by 50% to investigate a larger range of ΔV^*.

Figure 2 reports the average AoA along the blade span in the operating conditions of ~~Table~~ Tab. 1 and the maximum variation caused by the unsteady inflow associated with harmonic surge motion. Most of the blade sections work far from the stall front, and ~~the surge motion~~ surge-motion causes a variation of the AoA of some degrees. An additional set of 2D sectional model tests was carried out to characterize the unsteady aerodynamic behavior of the blade airfoil for a harmonic variation of the AoA. The amplitude and frequency of the latter covered the AoA variation experience by the full-turbine blades ~~because of the surge motion~~due to surge-motion.

3 The 2D experiments

2D sectional-model experiments were conducted at the DTU Red wind tunnel to characterize the SD7032 profile behavior in steady and unsteady conditions. Steady experiments, with fixed AoA, provided the airfoil polars for the range of Reynolds numbers ~~that is of interest for the blade of the wind turbine scale model~~explored in full-turbine tests. The experimental polars were used to ~~support the design of the scale model rotor, and to~~ define the conditions of the full-turbine experiment~~. Polars were also used for the~~ , and also for calibration of numerical models of the experiment ~~Cormier et al. (2018); Mancini et al. (2020).~~ (Cormier et al. (2018); Mancini et al. (2020)). Unsteady experiments, with harmonic variation of the AoA, gave an insight into the unsteady aerodynamics of the airfoil. ~~Results were used to support the design of the 3D experiment.~~ In the UNAFLOW

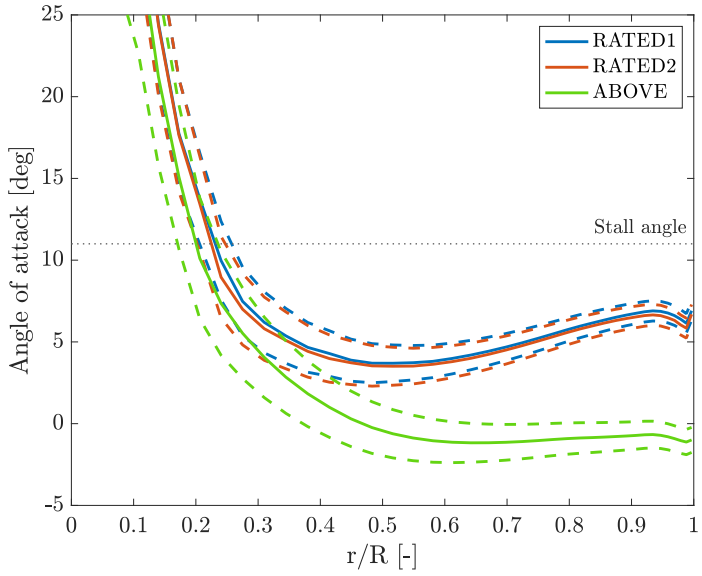

Figure 2. Average (solid lines) angle of attack along the span (r/R is the non-dimensional radial position) of the wind-turbine scale-model blade in the three operating conditions. The dashed lines in the corresponding colors show the maximum variation of the angle of attack because of the imposed surge motion.

project there ~~was not~~ wasn't a specific effort to reproduce ~~numerically~~ the unsteady airfoil behavior with numerical tools, however, a wide dataset of unsteady polars are provided as a project output. This data could be used both ~~to validate~~ for validation of unsteady airfoil aerodynamic models~~Boorsma and Caboni (2020)~~ , like it was done by Boorsma and Caboni (2020), or unsteady CFD ~~computation aiming to catch lift and drag oscillation due to dynamic variation of AoA.~~ computations.

The setup for 2D experiments is depicted in ~~Figure~~ Fig. 3. The 2D wing model, of 130mm chord, was fitted with a pressure loop (~~with~~ 32 taps) at midspan that was used to measure the lift force from the pressure distribution, and a single-component force transducer that provided an additional lift force gage. The profile drag was obtained by means of a down-stream wake rake. Two ESP 32HD pressure scanners from PSI pressure systems (±1psi and ±10"H2O range respectively) were connected to the airfoil and wake rake. The profile was mounted on a turning table that set the angle of attack.

3.1 Steady force coefficients

~~The force~~ Force coefficients were measured for chord Reynolds number ~~equal~~ of 50k, 60k, 75k, 100k, 150k, 200k and stepping through the AoA range from -10° to 25°. The Reynolds range covers the flow ~~condition~~ conditions experienced by the ~~blade of the wind turbine scale model (see Figure~~ turbine scale-model (see Fig. 1). Measurements were repeated in smooth flow (turbulence intensity lower than 0.1%), and with an increased free-stream turbulence that was obtained placing three thin wires (0.15mm diameter) about four chords upstream the profile. The slight increase in turbulence intensity ~~,~~ avoids the formation

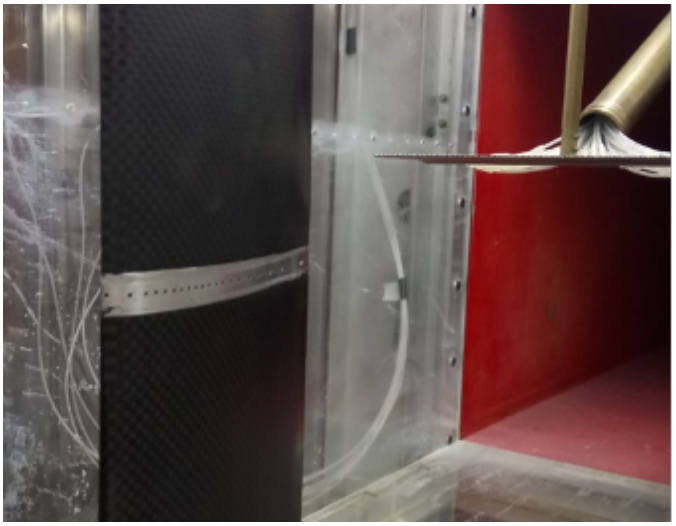

Figure 3. The experimental setup ~~that was~~ used to measure the blade polars in the DTU Red wind tunnel. The pressure loop is at the midspan of the blade sectional model, and the wake-rake is visible downstream.

of a laminar separation bubble by tripping the boundary layer. This inflow condition is deemed to be more realistic and closer to what is experienced by the ~~wind turbine scale~~ turbine model. The ~~lift and drag force coefficients are shown in Figure~~ airfoil pressure-lift and wake-drag coefficients are reported in Fig. 4. The lift coefficient shows a non-linear behavior in correspondence of the stall AoA, which is clearly present at Re 50k, and becomes less evident for increasing Re values. The increased turbulence results in a smoother drag coefficient~~for any Re value~~. The effect on the lift coefficient is to smear out the ~~non-linearity~~nonlinearity, and this is specially evident for Re values lower than 100k. The wake-drag measurement above 15 degrees is not reliable as the stalled wake covers the entire wake rake, thus airfoil pressure-based drag is used above stalled AoA. In general the SD7032 dependency for the Reynolds numbers considered, appears low for the lift between AoA 2-11 degrees. The linearity of lift is also good and drag does not show any nonlinearity making the SD7032 profile a well suited choice for a model-scale rotor in the Re-range 60-200k.

3.2 Unsteady force coefficients

The lift and drag force ~~coefficient~~ coefficients were also measured with ~~an unsteady pitching of the airfoil~~ unsteady airfoil pitching. The conditions of the 2D experiment reflected those of the full-turbine blade. The experiments investigated the profile behavior for chord-Reynolds number of 50k, 100k, 150k, and a static AoA of 0, 3, 6, 9, 10, 12, 15 degrees. The amplitude and frequency of the sinusoidal pitching reflects the AoA variation produced by the imposed ~~surge motion in the wind turbine scale model~~surge-motion in full-turbine tests. The AoA ~~amplitude was~~ amplitudes were 0.5, 1, 2, 5 and the ~~frequency of~~ frequencies 0.25, 0.5, 1, 2, 3 Hz.

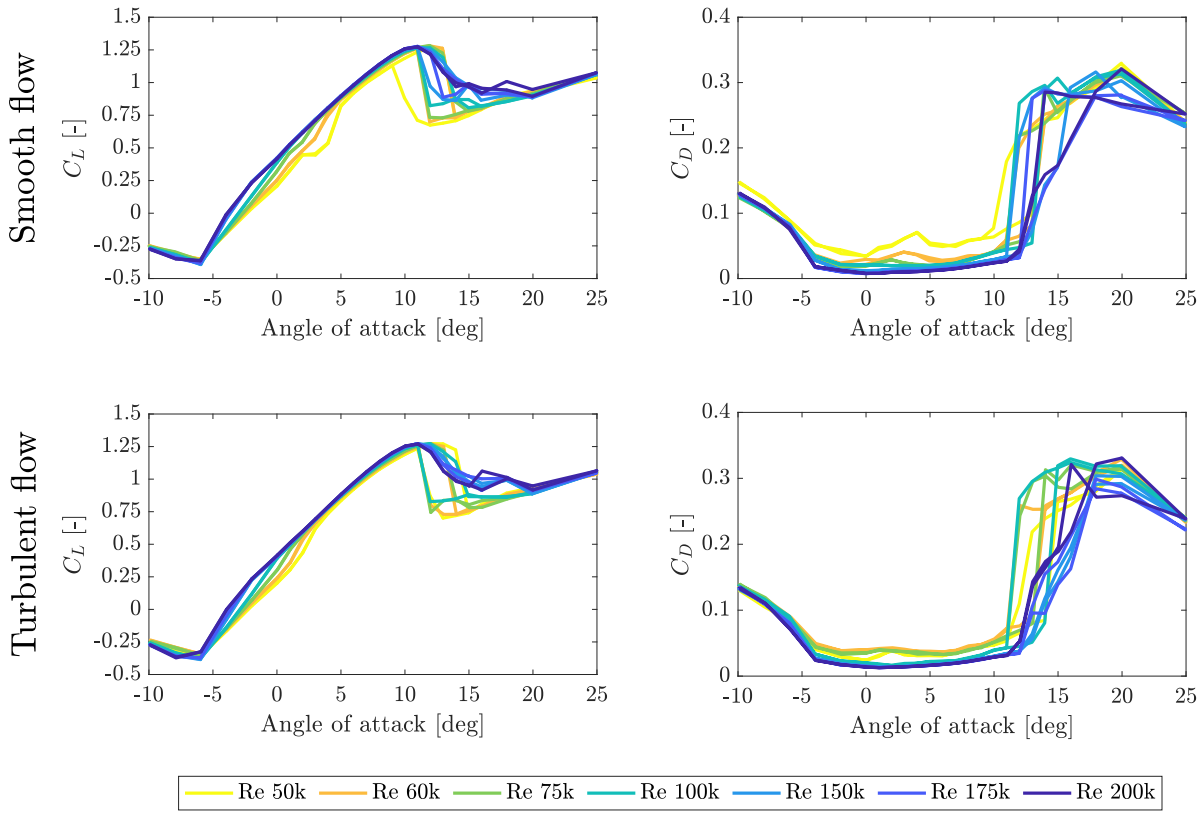

Figure 4. Steady lift (C_L) and drag (C_D) coefficients from 2D sectional model tests in smooth flow (top row) and with added turbulence (bottom row).

~~An example of the~~ A sample of results is reported in ~~Figure~~ Fig. 5, with reference to the inflow with increased turbulence, a chord Re of 50k, and a sinusoidal variation of the AoA of 5 degrees amplitude and different frequencies. ~~An~~ A hysteresis cycle is always present when the airfoil is pitched in correspondence of the stall AoA, and increasing the motion frequency, the strength of this effect is increased. The amplitude of the hysteresis cycle is instead small in the linear region (i.e., for AoA lower than the stall value), where most of the wind turbine model blade operates (see ~~Figure~~ Fig. 2).

4 The full-turbine experiments

The UNAFLOW experiments were carried out at the Politecnico di Milano wind tunnel (Galleria del Vento Politecnico di Milano ~~, GVPM ?~~GVPM). The facility is a closed-loop subsonic wind tunnel and the flow is generated by 14 fans. UNAFLOW tests were carried out in the low-speed test chamber, which has a cross section of 3.84x13.84 m.

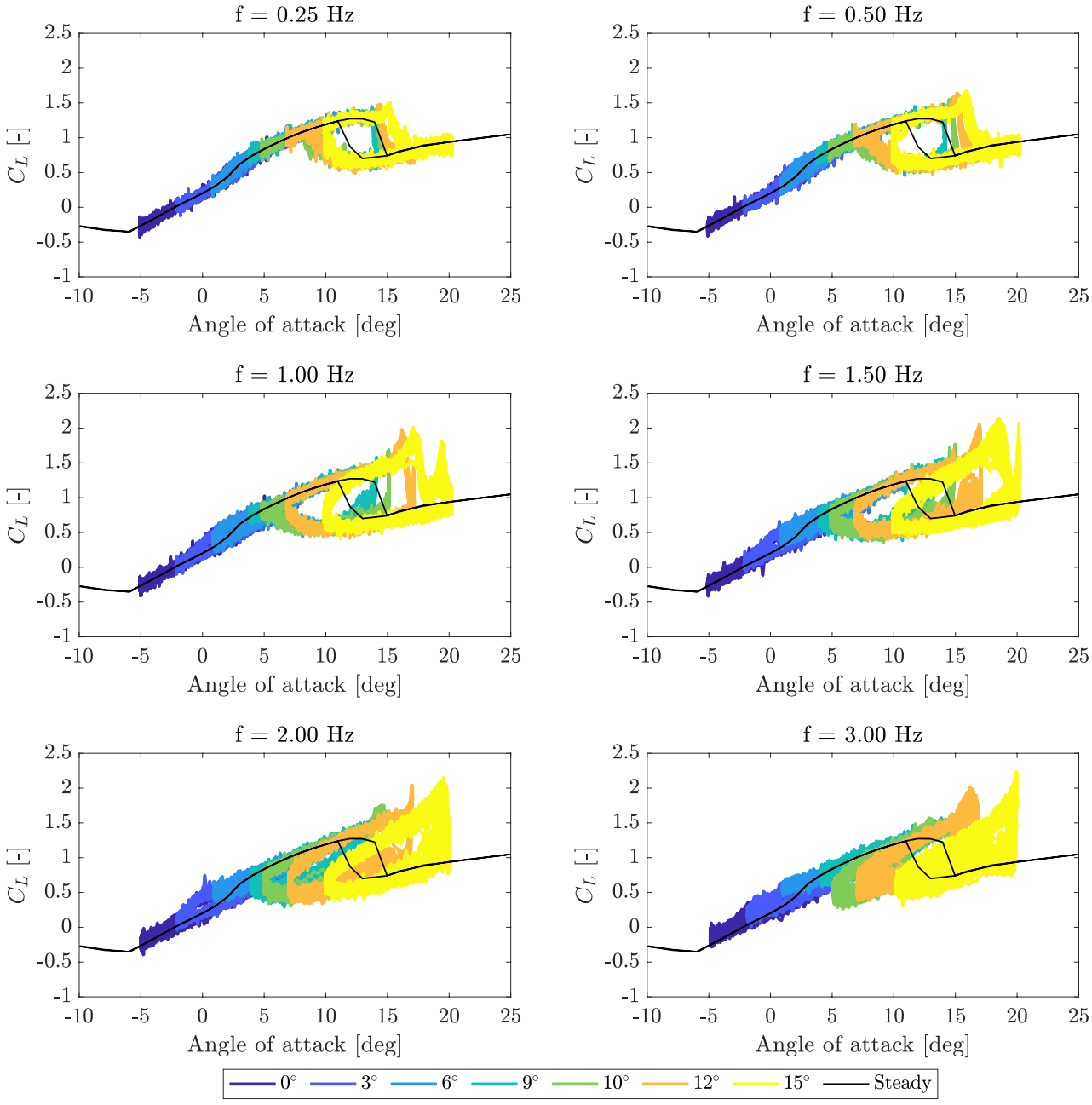

Figure 5. Unsteady lift coefficient (C_L) for a sinusoidal angle of attack variation of 5° and different frequencies, with ~~increased~~ turbulent inflow ~~turbulence~~ and a chord Re of 50k. ~~The color of~~ Colors denote the ~~dots denotes the~~ mean angle of attack, and the steady lift coefficient is reported in black.

The ~~wind turbine scale model was mounted~~ turbine scale-model was installed on the test rig shown in ~~Figure~~ Fig. 6. The test rig is formed by a slider ~~which is~~ driven by a ~~first~~ hydraulic actuator, and is utilized to simulate the ~~surge motion~~surge-motion. On top of the slider, there is a second hydraulic actuator ~~which is~~ connected to the base of the ~~wind turbine~~ tower through a slider-crank mechanism. The second actuator was utilized to tilt the wind turbine ~~so to have the rotor plane normal to the ground. In this way, the periodic effects due to the rotor tiltangle were avoided.~~ and make the rotor vertical (offsetting the rotor tilt).

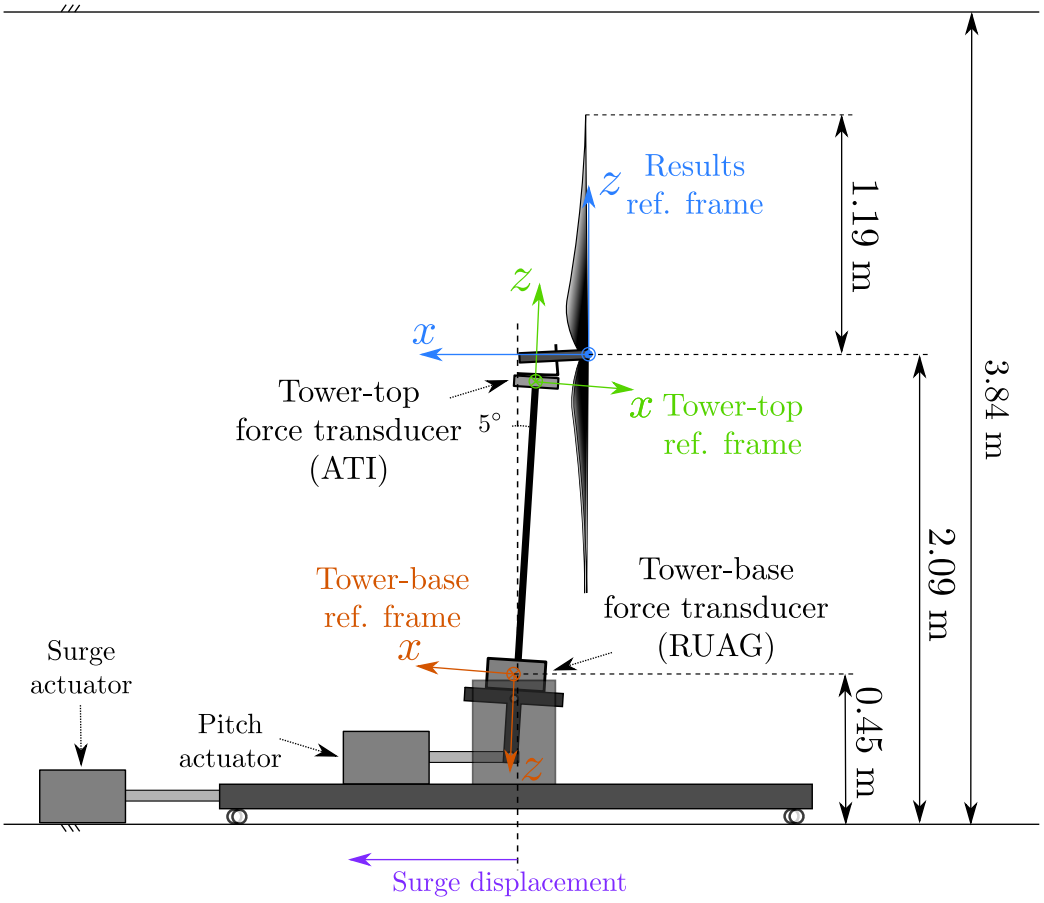

Figure 6. Schematic of the ~~wind tunnel~~ full-turbine test setup ~~, of the wind turbine scale model geometry,~~ and ~~the force transducers~~coordinate systems used for measurements and their analysis.

~~The experiment investigated three wind turbine operating conditions and several types of surge motion. The tested conditions are reported in Tables A1-A3, while the rationale behind their selection is explained in the rest of this section.~~

4.1 ~~The wind turbine scale model~~

The wind turbine ~~is a 1/75 scale model of the DTU 10MW Bak et al. (2013), that was designed within~~ scale model was originally designed by Bayati et al. (2017) for the LIFES50+ EU H2020 project~~Bayati et al. (2017)~~. The rotor ~~was designed based on the performance-scaling approach Kimball et al. (2014) to correctly reproduce the~~ design process is analyzed by Bayati et al. (2017b) and it is finalized at reproducing the thrust force coefficient of the full-scale reference wind turbine~~Bayati et al. (2017b)~~, according with the performance-scaling methodology (see Kimball et al. (2014)). The scale model specification are reported in ~~Table~~ Tab. 2.

Table 2. Specifications of the wind turbine scale model (RNA stands for rotor-nacelle ~~assembly~~assembly).

Parameter	Unit	Value
Rated wind speed	m/s	3.80
Rated rotor speed	rpm	240
Rotor diameter	m	2.38
Blade length	m	1.10
Hub diameter	m	0.18
Shaft tilt angle	deg	5.00
Blade mass	kg	0.21
Nacelle mass	kg	1.79
RNA mass	kg	3.58

4.1 Measurements

Several measurements were carried out during the ~~experiments~~experiment. The undisturbed wind velocity V was measured by a Pitot tube ~~that was located 5 m~~ 5m upstream the wind turbine, at 1.5m height from the floor. An LVDT sensor provided the feedback for the control system of the surge hydraulic actuator. In parallel, the wind turbine surge motion was measured by means of a MEL M5L/200 laser sensor. The tower-top forces were measured by a 6-components force transducer. Two PCB MEMS accelerometers were fixed in correspondence of the tower-base to measured the x and z acceleration; another two were mounted on the nacelle to measure the x and y acceleration. All instruments were sampled synchronously with a frequency of 2000 Hz. In few selected test cases, the wake of the wind turbine was scanned by tri-axial hot-wire probes. In an even smaller sample of test cases, PIV measurements were carried out to describe the wake flow structure.

4.2 ~~Tower-top~~ Rotor-integral aerodynamic forces

~~The six-components constraint force at the~~ Rotor-integral aerodynamic forces were evaluated from two load cells, one installed at tower-base (RUAG SG-Balance 192-6i) and one at tower-top ~~was measured by an~~ (ATI Mini45 SI-145-5~~force transducer.~~

~~Such measurements cannot be used directly to evaluate the aerodynamic forces because they also include the rotor-nacelle assembly (RNA)weight and inertia. To isolate the aerodynamic fraction of the force measurement, another set of tests was carried out.~~). The two sensors and the coordinate systems utilized for force measurements are depicted in Fig. 6. Aerodynamic loads are obtained removing the inertial and weight components from force measurements. Each motion condition of the wind tests (SIW) of ~~Tables~~ Tab. A1-A3 was tested without wind and with fixed rotor (NOW). In the NOW tests, ~~only~~ the output of the tower-top sensor is only the inertia and weight ~~forces were measured.~~

~~The experiment focused on the thrust force, because it is a driving load in FOWTs. The aerodynamic thrust force was obtained according to this procedure, which is based on the assumption that the structural loads depend only on the type of motion and are the same in the NOW and SIW tests:~~ of the rotor-nacelle assembly. Aerodynamic forces are then obtained subtracting NOW measurements from SIW measurements:

1. for any given motion condition, the SIW time histories are synchronized with the corresponding NOW~~. The reference signal for the procedure is the LVDT position;~~ ;
2. SIW and NOW time histories are trimmed, keeping the maximum number of full periods of motion;
3. the aerodynamic forces are obtained subtracting the NOW time series from the SIW time series:

$$F_{a,i}(t) = F_{SIW,i}\mathrm{SIW},_i(t) - F_{NOW,i}\mathrm{NOW},_i(t) \qquad i = 1,\ldots,6\,. \tag{5}$$

~~The procedure strongly~~ The force-subtraction procedure relies on the ~~assumption that~~ rigid-body assumption for the tower and blades~~behave as rigid bodies~~, hence structural loads depend only on the type of motion and are the same in the NOW and SIW tests. This is ~~in general true around the frequency of the imposed surge motion, which was in any case~~ valid when the surge-motion frequency is lower than the natural frequencies of the wind turbine components and, in particular, of the first ~~tower fore-aft mode(6.5 Hz)~~FA mode. For higher motion frequencies, the dynamic amplification associated with tower flexibility cannot be neglected~~anymore, and the~~ , and results obtained based on the inertia-subtraction procedure ~~are not reliable. In Mancini et al. (2020), an alternative inertia-subtraction algorithm is proposed to better deal with tower flexibility.~~ may be unreliable. Flexibility of turbine-model components is a source of uncertainty for the experiment, but its quantification was outside the scope of the UNAFLOW test campaign. An additional test campaign is currently planned to address this specific issue.

4.3 Hot-wire wake measurements

An automatic traversing system was ~~used~~ utilized to measure the three-component velocity in ~~the wake of the wind turbine~~ turbine model wake. The system, ~~visible in Figure~~ depicted in Fig. 7, consists of a moving arm mounting two hot-wire probes. Measurements were carried out with the traversing system spanning across the Y-Z plane (cross-wind, CW) or ~~across~~ the X-Z plane (along-wind, AW) ~~.~~

of the "Results ref. frame" of Fig. 6. In the CW case, the measurement plane was 2.3D (5.48 m) downwind the ~~wind turbine; this~~ turbine. This was the furthest distance ~~given~~ allowed by the size of the ~~test chamber~~ wind-tunnel test chamber, and it is

~~considered to be~~ part of the near-wake region ~~Vermeer et al. (2003)~~(Vermeer et al. (2003)). One of the probe was mounted at hub-height, the other 0.2 m below. The probes were moved in the cross-wind direction, ranging from -1.6 m to 1.6 m with respect to the hub position, with a distance of 0.1 m between subsequent points. CW measurements were carried out both for the ~~Rated2 and Above~~ RATED2 and ABOVE conditions, with and without surge motion.

In the AW case, the two probes were mounted at hub-height, one next to the other: the first at y = 0.7 m, the second at y = 0.9 m. The probes were moved in the along-wind direction, ranging from 2.18 m to 5.48 m downwind the hub location, with a distance of 0.33 m between subsequent points. AW measurements were carried out only for the ~~Rated2~~ RATED2 condition, with and without ~~surge motion.~~

surge-motion.

Figure 7. Test setup for along-wind (AW) hot-wire measurements (left) and PIV (right) measurements.

4.4 PIV wake measurements

A PIV system was used to investigate a portion of the X-Z plane in the near-wake region. The PIV system ~~encompasses~~ is made of an Nd:YAG double pulsed laser and two adjacent cameras, mounted on a traversing system, with a line of sight perpendicular to the laser sheet. The measurement area ranged from 0.6 m to 1.35 m downwind the hub location, and from 0.6 m to 1.39 m from the hub in the vertical direction. The image pairs were post-processed ~~using~~ with PIVTEC PIVview 3C. PIV measurements were carried out for the ~~Rated2~~ RATED2 condition, with and without surge motion.

~~For the tests without surge motion~~For tests without surge-motion, measurements were phase-locked to the blade-1 azimuth position (ψ). 100 image pairs were acquired for each measurement, from $\psi = 0°$ to $\psi = 120°$ with a $15°$ step, and from from $\psi = 120°$ to $\psi = 360°$ with a $30°$ step.

~~For the tests with surge motion~~For tests with surge-motion, only the motion conditions with a frequency which is ~~an~~ integer sub-multiple of the rotor frequency (i.e., 4 Hz) were considered. Measurements were phase-locked to the surge position, and image pairs were acquired in several points of the motion cycle. Being the rotor frequency an integer multiple of the surge frequency, the blade-1 azimuth position is the same for ~~all the measurements~~ any measurement in a given surge position.

5 Key findings of the full-turbine ~~experiments~~experiment

This section reports the key findings of the full-turbine experiment. First, rotor-thrust force measurements are compared to the prediction of a quasi-steady model for several harmonic surge-motions. Rotor-thrust affects the along-wind response of the floating turbine, and is in turn affected by its motion (i.e., it is a state-dependent force). A correct prediction of thrust-force response to turbine motion is therefore important when assessing the global dynamics of an FOWT. Second, the effects of surge-motion on the turbine near-wake are investigated by means of hot-wire measurements. Spectral analysis reveals how surge-motion affects the wake energy content. Last, PIV measurements of the wake area near the rotor show the effect of turbine translation on the blade-tip vortex.

5.1 Rotor thrust force

~~The analysis of the thrust force~~ Tower-top force measurements are analyzed to investigate the thrust-force response to surge-motion. The analysis is based on a simplified description of the wind turbine rotor, ~~that focus on the~~ which focusses on integral forces rather than ~~considering the single blades. The~~ single-blade loads. According to this model, the rotor produces a thrust force:

$$T = \frac{1}{2}\rho\pi R^2 C_T V^2\,, \tag{6}$$

where ρ is the air density, R the rotor radius, C_T the thrust coefficient and V the undisturbed wind speed. The thrust coefficient is set by the ~~wind~~ turbine operating condition, which is defined by the TSR λ and the collective pitch angle β:

$$C_T = C_T(\lambda, \beta), \qquad \lambda = \frac{\omega R}{V}\,. \tag{7}$$

The thrust force can be linearized based on a first-order Taylor expansion:

$$T \simeq T_0 + K_{VT}\Delta V + K_{\beta T}\Delta\beta + K_{\omega T}\Delta\omega\,, \tag{8}$$

where T_0 is the steady-state thrust force; ΔV, $\Delta\beta$ and $\Delta\omega$ are the variation of ~~rotor~~ wind speed, collective pitch angle and ~~wind~~ rotor speed from their respective steady-state value; K_{VT}, $K_{\beta T}$ and $K_{\omega T}$ are the partial derivatives of thrust with respect to wind speed, collective pitch and rotor speed ~~Bianchi et al. (2007)~~(the definition is reported for example in Bianchi et al. (2007)). In the present case, collective pitch and rotor speed are fixed, so:

$$T \simeq T_0 + K_{VT}\Delta V\,, \tag{9}$$

with:

$$K_{VT} = \frac{T_0}{V}\left(2 - \frac{\partial C_T}{\partial \lambda}\bigg|_0 \frac{\lambda_0}{C_{T,0}}\right), \tag{10}$$

where λ_0 is the steady-state TSR and $C_{T,0}$ the steady-state thrust coefficient.

The wind speed seen by any point of the rotor when the ~~flow is smooth and the wind turbine moves in the surge direction is:~~ wind turbine undergoes a surge-motion is:

$$V = V_0 - \dot{x}, \qquad \Delta V = -\dot{x}\,, \tag{11}$$

where V_0 is the mean wind speed. The thrust force is:

$$T \simeq T_0 - K_{VT}\dot{x}, \qquad \Delta T = -K_{VT}\dot{x}\,. \tag{12}$$

The thrust force variation induced by the ~~surge motion~~ surge-motion is predicted based only on the wind turbine steady-state operational data. Equation 12 is therefore ~~herein~~ referred to as quasi-steady theory. According to quasi-steady theory (QST), the thrust force variation depends only on ~~the~~ surge velocity.

The focus of ~~the experimental~~ force measurements is the surge-frequency ~~thrust force . At the surge frequency, the effects of tower flexibility are small, and the thrust force is~~ aerodynamic-thrust force component, extracted from the tower-top force measurements based on the inertia-subtraction procedure presented in ~~Section~~ Sec. 4.2. The surge-frequency thrust force is:

$$\Delta T = |\Delta T| e^{j\phi}\,, \tag{13}$$

where $|\Delta T|$ is the amplitude of ~~the~~ thrust force at the surge frequency and ϕ is the phase with respect to the surge displacement. In general, the surge-frequency thrust force has a component in opposition of phase to ~~the~~ surge velocity, and one in opposition of phase to ~~the~~ surge acceleration. According to the QST model of Equation 12, ~~the~~ thrust force is perfectly ~~in aligned to the~~ aligned to surge velocity.

The adherence of ~~the~~ thrust force measurements to the QST model is ~~studied based on the unsteady thrust force~~ verified looking at the unsteady thrust-force coefficient:

$$C_{\Delta T} = \frac{\Delta T}{\frac{1}{2}\rho\pi R^2 V^2}\,. \tag{14}$$

This non-dimensional representation is ~~useful~~ also useful to ease the comparison of experimental results to ~~make the outcomes of the experiment comparable to~~ other studies. According to the QST:

$$|\Delta T| = 2\pi f_s A_s K_{VT}\,, \tag{15}$$

and the unsteady thrust coefficient is:

$$C_{\Delta T}^{QST} = 2\pi f_r A_r C_0^*\,, \tag{16}$$

where $f_r = 1/V^*$ is the reduced surge-frequency, $A_r = A_s/D$ the reduced surge-amplitude, and:

$$C_0^* = \left(C_{T0} \left(2 - \frac{\partial C_T}{\partial \lambda} \bigg|_0 \frac{\lambda_0}{C_{T0}} \right) \right). \tag{17}$$

~~The~~ The experimental unsteady thrust coefficient for ~~the motion conditions investigated in the experiment is shown~~ several surge-motion conditions is reported on the left of ~~Figure 8. In the figure~~ Fig. 8 as a function of f_r (notice that $C_{\Delta T}$ is divided by A_r ~~and is reported as function of f_r. In this plot, the QST prediction corresponds to a straight line, which slope is set by the wind turbine operating condition and the steady-state thrust characteristic. The dashed linesare~~), and the thrust-force phase is shown on the right of the same figure. Measurements are compared to the QST predictions, which correspond in the plot to straight lines, obtained as in ~~Equation 16based on steady-state thrust coefficient of the wind turbine scale model Belloli et al. (2020) . The phase of the thrust force is shown on the right of Figure 8.~~ Eq. 16. The QST prediction depends the turbine operating condition and its steady-state thrust coefficient characteristic. According to QST, the phase is -90°, regardless of the motion condition ~~. For low values of f_r the~~ and wind speed. Measurements where the surge-motion frequency was higher than 1.5 Hz were discarded from the analysis, to exclude any effect of tower flexibility. Uncertainty due to tower flexibility is not quantified, but is deemed small for imposed surge-motion frequencies below 1.5 Hz. For small values of reduced frequency, thrust force measurements ~~follow the QST~~ are aligned to QST predictions. For increasing values of ~~f_r, the thrust force has a small component in phase with the surge position, which is not predicted by QST. This is visualized by the phase ϕ, which increases above -90°, and by~~ reduced frequency, $C_{\Delta T}$ ~~, which shifts~~ appears to progressively shift away from the QST line~~. A trend appears in $C_{\Delta T}$, but it is less evident in~~ , with a trend that is consistent for data of the RATED2 and ABOVE cases. The same trend cannot be easily identified in the phase ϕ, ~~which is~~ as data are scattered in a range of $\pm 10°$ around -90°. ~~This uncertainty~~ The uncertainty in phase data is related to the ~~fact that part of the thrust force~~ thrust force component opposed to the surge acceleration ~~is in any case very small , and difficult to measure.~~ which is responsible of phase deviations. This force component is small and difficultly measured, thus the uncertainty for phase data is greater than for $C_{\Delta T}$. Analysis of uncertainty related to the turbine model flexibility may help discerning wether the deviation of data from QST for increased surge-motion frequency is due to tower flexible dynamics or rotor aerodynamic response.

5.2 Hot-wire wake measurements

The wake shape at hub-height is captured by the mean velocity deficit. The deficit for all the conditions that were investigated with hot-wire measurements is shown in ~~Figure~~ Fig. 9. The reduction of axial velocity is always higher ~~in~~ for RATED2, where the wind turbine is operated at ~~the~~ maximum power coefficient, compared to ABOVE. The wake is also slightly asymmetric with respect to the hub. For any condition the velocity deficit is larger on the left side compared to the right. When the wind turbine moves, the wake is slightly narrower, meaning there is more energy in its outer region. Outside the ~~boundaries of the rotor , a certain speed up~~ rotor boundaries, a speed-up is observable, which is caused by the wind tunnel blockage. Concerning the surge motion, it appears evident that it does not significantly change the mean wake deficit. Even if there are some major differences in the experiment (a porous disk was used to emulate the wind turbine rotor, measurements were carried out at a

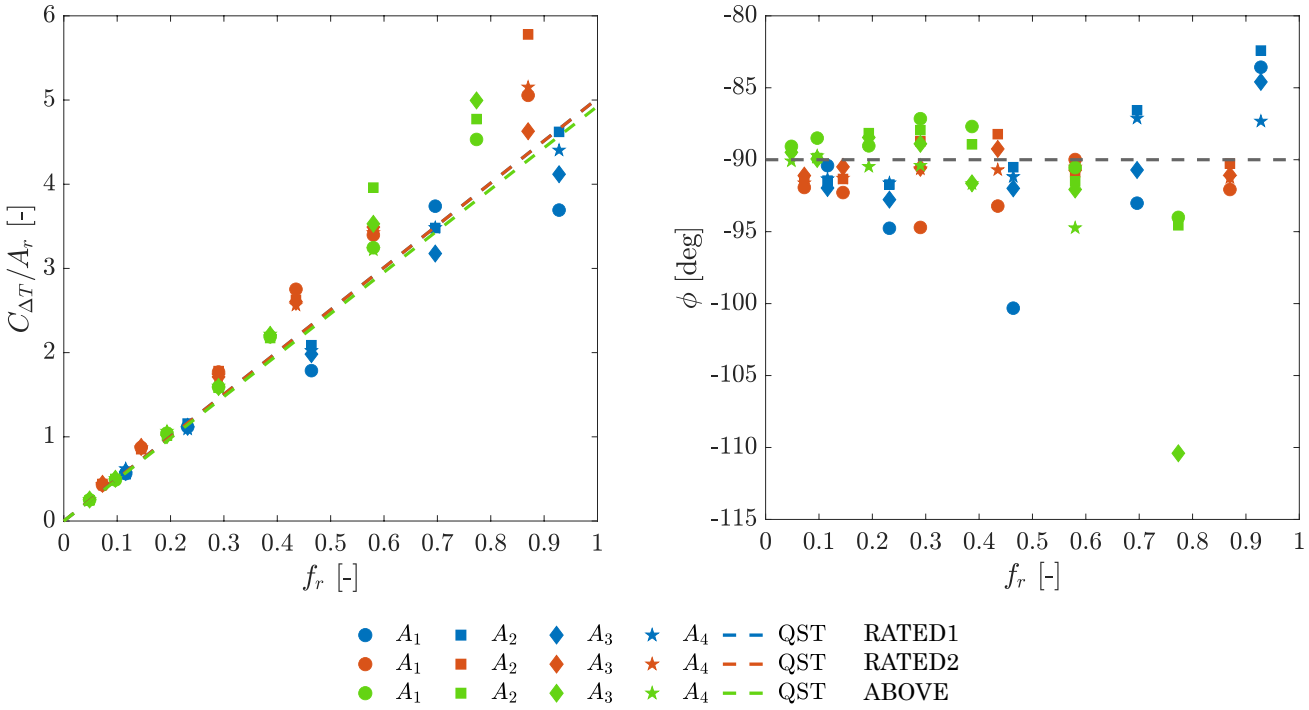

Figure 8. ~~Left: unsteady~~ Unsteady thrust coefficient ~~against reduced frequency; right:~~ (left) and phase of the ~~thrust force~~ thrust-force with respect to ~~the surge motion~~ surge-motion (right) against reduced frequency. ~~RATED1 (blue)~~Color is for mean wind speed, ~~RATED2~~ marker for surge amplitude (~~orange~~)e.g., ~~ABOVE (green~~for RATED1 and $f_r = 0.928$, $\bullet = 0.008$m, $\blacklozenge = 0.015$m, $\blacksquare = 0.025$m, and $\bigstar = 0.030$m, see Tab. A1-A3), dashed line for quasi-steady theory ~~(dashed lines)~~prediction.

distance of 4.6D, the inflow was turbulent), this is in agreement with Schliffke et al. (2020), where it is evidenced that ~~the surge motion~~ surge-motion does not affect the shape of the vertical wake profile.

The ~~frequency content of the wake~~ wake frequency content at hub-height is studied plotting the PSD of the three velocity components ~~measured~~ in different points across the rotor. Figure 10 compares the spectral plots for the RATED2 case without and with surge motion, in particular with reference to the case of ~~$f = 1\ Hz, A = 0.035\ m$~~ $f = 1$ Hz, $A = 0.035$ m. The energy content is concentrated in the outer region of the rotor and it is reasonably related to the blade-tip vortex. This distribution of energy is common also to any ~~other~~ RATED2 case. The asymmetry seen in the velocity deficit is found also in the spectra, and it is particularly evident in the vertical component~~W~~, which is associated with ~~the rotor angular speed~~rotor spinning. Looking at the unsteady case, a strong harmonic component is visible at the frequency of motion, which is absent in the steady case. The surge-frequency harmonic is more evident in the axial velocity, compared to the other two velocity components. Another strong harmonic component is visible close to ~~$f = 4\ Hz$~~ $f = 4$ Hz, the 1P frequency, and it is associated with ~~a slightly different pitch angle setting for the three blades.~~ aerodynamic and mass imbalance.

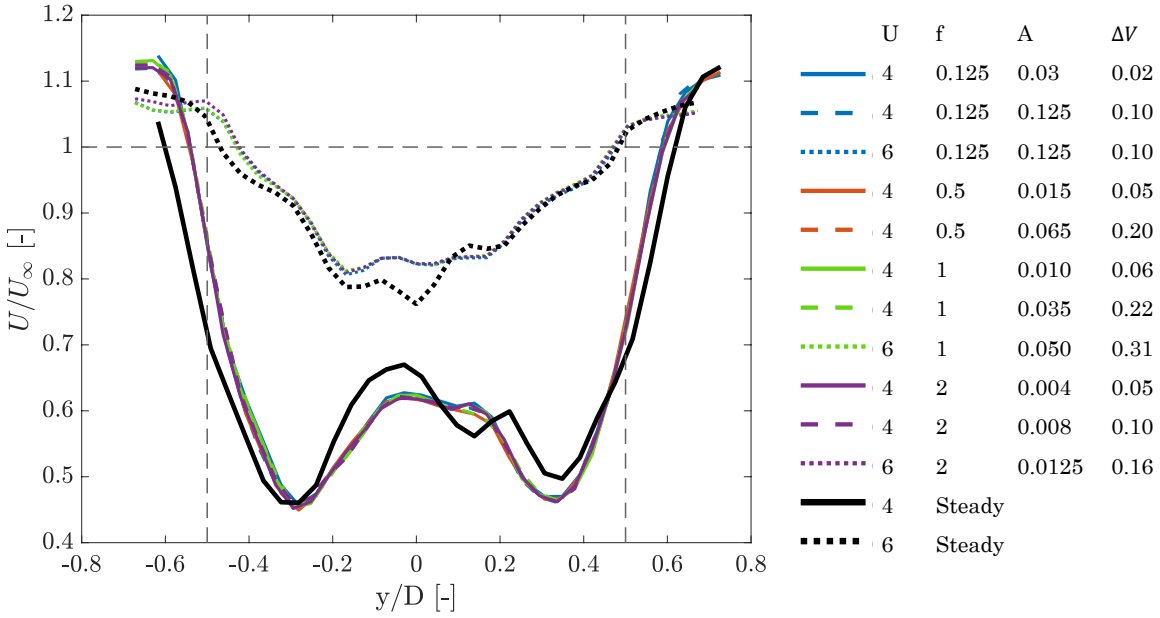

Figure 9. Mean velocity deficit at hub-height ($y = 0$ corresponds to the hub location, the rotor edge is marked by the vertical ~~dotted~~ dashed lines) for the steady cases (i.e., without surge motion) and unsteady cases. In the legend: U is the mean wind speed, f the surge frequency, A the surge amplitude, ΔV the maximum surge velocity.

The same analysis is carried out in ~~Figure~~ Fig. 11 for what concerns the ABOVE condition. In this case, energy is concentrated in the inner region of the rotor, witnessing the presence of a strong blade-root vortex. Also in this case, the 1P component is visible, at ~~$f = 4.417\ Hz$~~ $f = 4.417$ Hz and the wake is slightly asymmetric. In ~~the case with surge motion~~case of surge-motion, an harmonic ~~becomes evident~~ is visible at the surge frequency. The harmonic is equally present in the three velocity components.

~~It is possible to have a more detailed description of the effect of the surge motion on the wake looking at two PSD functions. The analysis is carried out for~~ More information about the surge-motion effect on wake is provided by two additional metrics obtained from the from the PSD of the axial velocity~~component, since it is aligned with the surge direction and it is most affected by the wind turbine motion.~~ . The space-averaged PSD gives a description of the energy distribution in frequency and it is obtained summing the PSD for all the measurement points (i.e., summing across the x-axis of Fig. 10-11):

$$\overline{U}_f = \frac{\sum_{y=1}^{n_y} U_{y,f}}{\sum_{y=1}^{n_y} \sum_{f=1}^{n_f} U^0_{y,f}}, \tag{18}$$

where $U_{y,f}$ is the PSD of the axial velocity at point y evaluated at frequency f, n_y is the number of points where the wake speed is measured, and n_f the number of discrete frequencies where the PSD is computed. $U^0_{y,f}$ denotes the PSD for the steady case with the same mean wind speed of $U_{y,f}$. ~~This choice, allows to understand how the wake energy content changes because of the surge motion.~~ The space-averaged PSD $\overline{U}_f$ for the investigated conditions is shown in ~~Figure~~ Fig. 12. In the steady

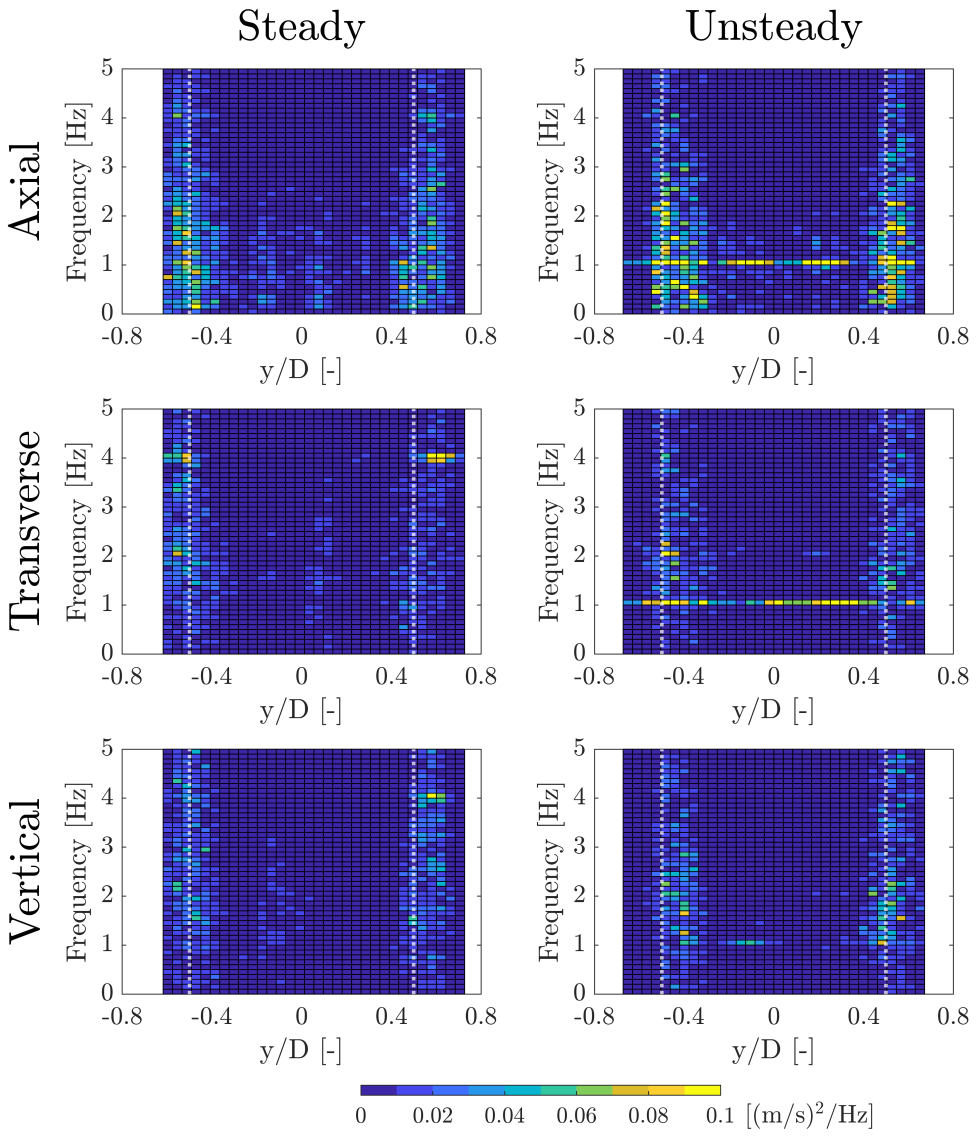

Figure 10. PSD of the hub-height wake velocity components ~~(*U* axial, *V* lateral, *W* vertical)~~ in ~~different~~ several cross-wind positions (~~*y* = 0~~ *y*/*D* = 0 corresponds to the hub location, ~~the~~ rotor edge is marked by the vertical dotted lines) for the RATED2 case. ~~Top: steady condition; bottom:~~ The surge-motion of the unsteady ~~condition~~ case is with ~~*f* = 1 *Hz*~~ *f* = 1 Hz, ~~*A* = 0.035 *m*~~ *A* = 0.035 m.

455 case, energy is evenly spread below 1 Hz, and decreases smoothly increasing frequency. A peak is always present at the 1P frequency. The energy is greater in RATED2 compared to ABOVE, and also the 1P peak for the above cases is much lower than for the RATED2 cases. The spectrum for any ~~of the unsteady cases is similar to the spectrum of the~~ unsteady case is similar in the corresponding steady case, except for a peak at the surge frequency~~.~~. This suggests that some energy is transferred in the wake by the ~~surge~~ turbine motion. Similar findings, but for the far-wake of a porous disk, are reported ~~in~~ by Schliffke et al.

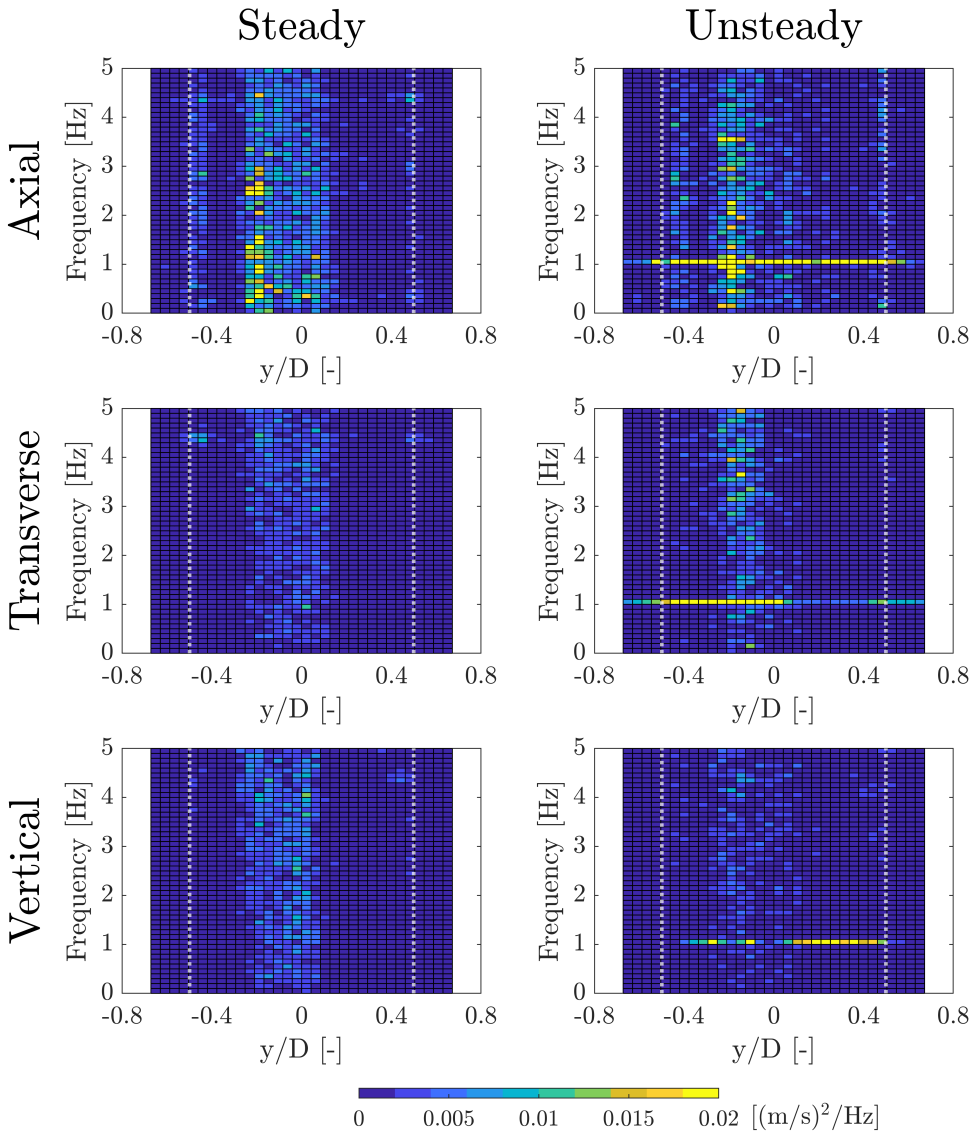

Figure 11. PSD of the hub-height wake velocity components ~~(*U* axial, *V* lateral, *W* vertical)~~ in ~~different~~ several cross-wind positions (~~$y = 0$~~ $y/D = 0$ corresponds to the hub location, ~~the~~ rotor edge is marked by the vertical dotted lines) for the ABOVE case. ~~Top: steady condition; bottom:~~ The surge motion of the unsteady ~~condition~~ case is with ~~$f = 1$ Hz~~ $f = 1$ Hz, ~~$A = 0.05$ m~~ $A = 0.05$ m.

460 (2020). Looking at the PSD of ~~Figure~~ Fig. 12 it is also interesting to notice that, for a surge frequency up to 1 Hz, the amplitude of the surge-frequency peak is proportional to ΔV, but not linearly. The energy increment in the 2 Hz case is much lower than for any other motion condition with similar ΔV. The ~~surge motion~~ surge-motion also amplifies the 1P harmonic and the amplification in RATED2 is ~~much higher~~ greater than in ABOVE ~~conditions~~condition.

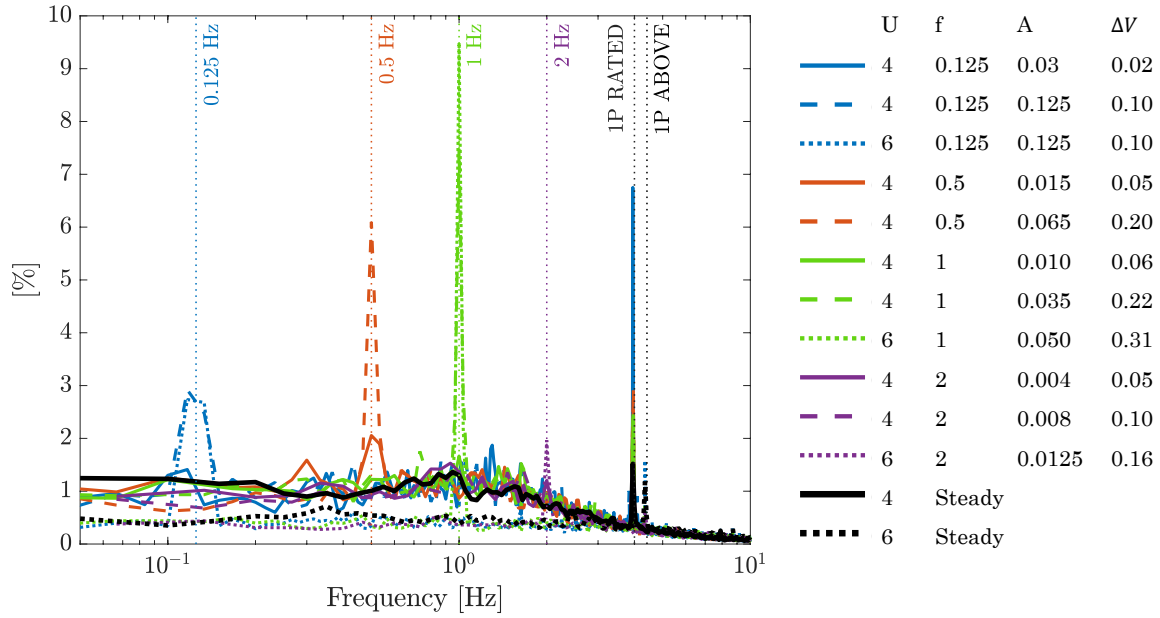

Figure 12. Space-averaged PSD of the hub-height axial velocity for different frequencies. The vertical dotted lines mark the frequencies of surge motion and the rotor frequency. In the legend: ~~U~~ U is the mean wind speed, ~~f~~ f the surge frequency, ~~A~~ A the surge amplitude, ΔV the maximum surge velocity.

The frequency-averaged PSD ~~defines~~ describes how energy is distributed across the rotor and it is computed, for any measurement point, as the frequency-integral of the corresponding PSD (i.e., summing across the y-axis of Fig. 10-11):

$$\overline{U}_y = \frac{\sum_{f=1}^{n_f} U_{y,f}}{\sum_{y=1}^{n_y} \sum_{f=1}^{n_f} U_{y,f}} \,. \tag{19}$$

In this case, $U_{y,f}$ is used for normalization. The frequency-averaged PSDs $\overline{U}_y$ are reported in ~~Figure~~ Fig. 13. The energy space distribution is not affected by the ~~type of~~ turbine motion, and it is strictly characteristic of the operating condition. In RATED2 conditions, energy is concentrated in the outer region of the rotor and it is associated with the blade-tip vortex. In ABOVE ~~conditions~~condition, most of the energy is in the central part of the rotor, where the blade-root vortex is, whereas the contribution of the tip vortex is lower. More energy is present on the left than on the right of the hub and this is particularly evident in the ABOVE cases. ~~The fact the shape of $\overline{U}_y$ remains the same, suggests the surge motion adds energy evenly across the rotor. In detail, it~~ Energy is increased across the entire rotor, but the increment is more consistent in correspondence of the blade-tip for RATED cases, and the blade-root for ABOVE cases. This suggest that sure motion increases the axial travel velocity of ~~vortices.~~ the blade-tip and blade-root vortices.

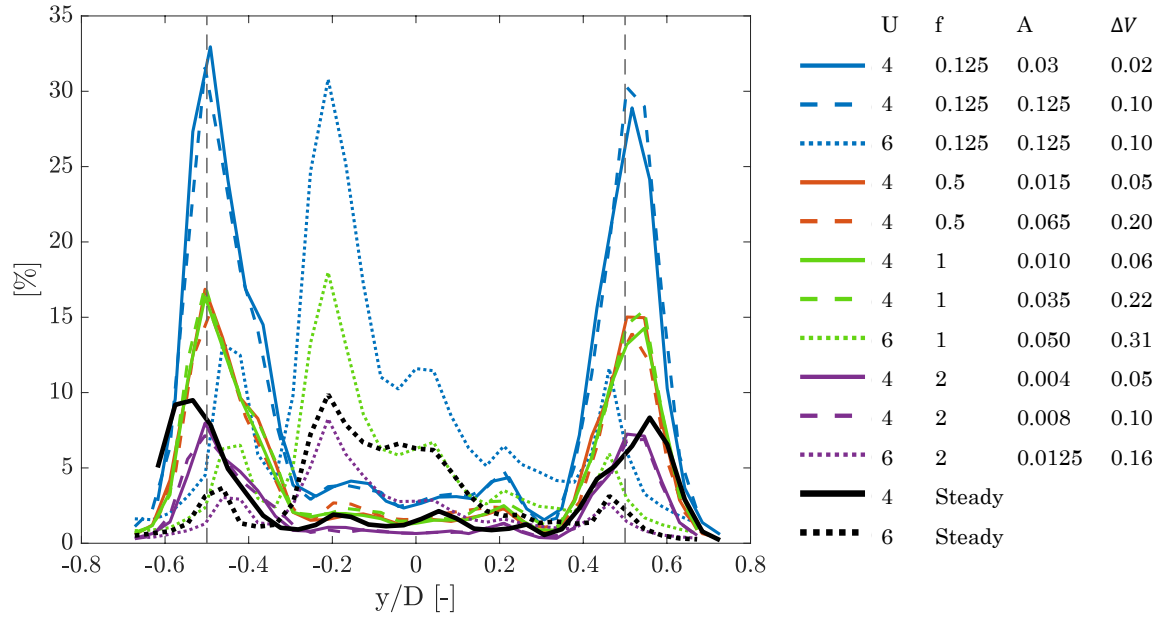

Figure 13. Frequency-averaged PSD of the hub-height axial velocity in different cross-wind positions (~~$y = 0$~~ $y/D = 0$ corresponds to the hub location, the rotor edge is marked by the vertical ~~dotted~~ dashed lines). In the legend: ~~U~~ U is the mean wind speed, ~~f~~ f the surge frequency, ~~A~~ A the surge amplitude, ΔV the maximum surge velocity.

5.3 PIV wake measurements

PIV combined with a realistic ~~wind turbine scale model , makes it possible~~ turbine model allows to appreciate the ~~structure of the wind turbine wake and investigate how it is~~ wake flow-structures and to investigate how these are affected by the ~~surge motion~~ motion of the structure. The focus of the analysis is on the blade-tip vortex~~as it holds most~~ , because it holds a significant fraction of the wake energy, as seen from hot-wire measurements.The blade-tip vortex is visualized ~~by means of the magnitude of the vorticity , obtained from the in-plane velocity components~~(u, v)~~.~~

from the vorticity magnitude, computed based on the transverse and vertical velocity components. Figure 14 reports the vorticity magnitude for the ~~portion of the investigation area that contains the~~ area of the wake near blade-tip~~vortex~~. The flow field was measured in RATED2 conditions without surge motion with a blade-1 azimuth of zero degrees. The tip-vortices shed by the blades are clearly seen. The vortices position does not change for subsequent PIV images captured in the same azimuthal position of blade-1.

Figure 15 shows the vorticity magnitude in the same condition, but with a ~~surge motion of frequency~~ surge-motion frequency of 1 Hz and amplitude of 0.065 m. PIV images are acquired in eight different surge positions ~~and~~ for a blade-1 azimuth of zero-degrees. The ~~position of the~~ tip-vortices position is modified by the ~~presence of the surge~~ turbine motion, and ~~it~~ varies periodically with the ~~surge motion frequency.~~ frequency of surge motion. The mechanism behind ~~the evolution of the wake~~

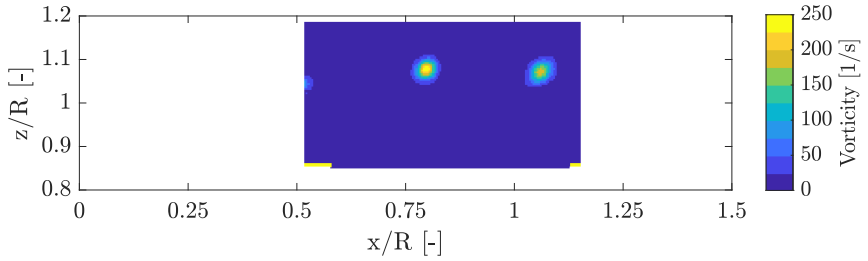

Figure 14. Vorticity for the RATED2 operating condition without surge motion. x/R and z/R are the axial and vertical distance from rotor ~~rotor~~ apex normalized by rotor radius. The origin of the axes is coincident with the rotor apex when the wind turbine is in the zero-surge position (see the Results ref. frame of Fig. 6).

wake evolution is explained comparing two phases of the surge motion with equal but opposite velocity (e.g., phase 4 and phase 8 in ~~Figure~~ Fig. 15). When the rotor moves with a downwind velocity (phase 4), the tip vortices are released with a lower velocity than without ~~surge motion~~ surge-motion and travel a lower distance in the wake~~; the~~ . The opposite is true when the rotor moves with an upwind velocity (phase 8). This mechanism ~~explains the increase of the surge-frequency energy content of the wake~~ can explain the increased wake energy content seen in hot-wire measurements. An algorithm for detection of vortex position and size, like those presented by Chakraborty et al. (2005), may be used in future to quantify the effect of surge-motion on the blade-tip vortex travel speed. The behavior of the tip vortex was studied by means of CFD simulations ~~in~~ by Cormier et al. (2018) with similar findings. Numerical simulations ~~also~~ show a stable vortex merging which is not evidenced by the experiment.

6 Conclusions

This ~~paper presented~~ article presented an extensive wind-tunnel experiment for the unsteady aerodynamic response of a floating wind turbine subjected to surge motion. The low-Reynolds airfoil of the ~~UNAFLOW experiments. Advanced wind tunnel measurements were carried out to improve knowledge about the unsteady aerodynamics of floating offshore wind turbines. Data were also produced to be a reference for the validation of numerical codes.~~

~~Thrust force plays a crucial role in floating wind turbine, as it drives the dynamic response of the platform surge and pitch modes. The thrust force was investigated by means tower-top force measurements . The thrust force measurement for several surge-motion conditions is compared to the prediction of~~ turbine-model blade was characterized in a dedicated 2D experiment, in steady and unsteady conditions. The steady lift force coefficient has a linear behavior for AoA between -5 and +8 degrees. A hysteresis cycle is present in correspondence of the stall AoA, when the airfoil is subjected to sinusoidal pitching, and extends to lower AoAs for increasing pitching frequency. Knowledge about the airfoil response is leveraged to select the wind and motion conditions of the full-turbine experiment. Three wind speeds are selected: two are representative of below-rated operations, where the blade is operated at high AoA, one of above-rated operations, where the blade pitch angle is lower. The turbine model

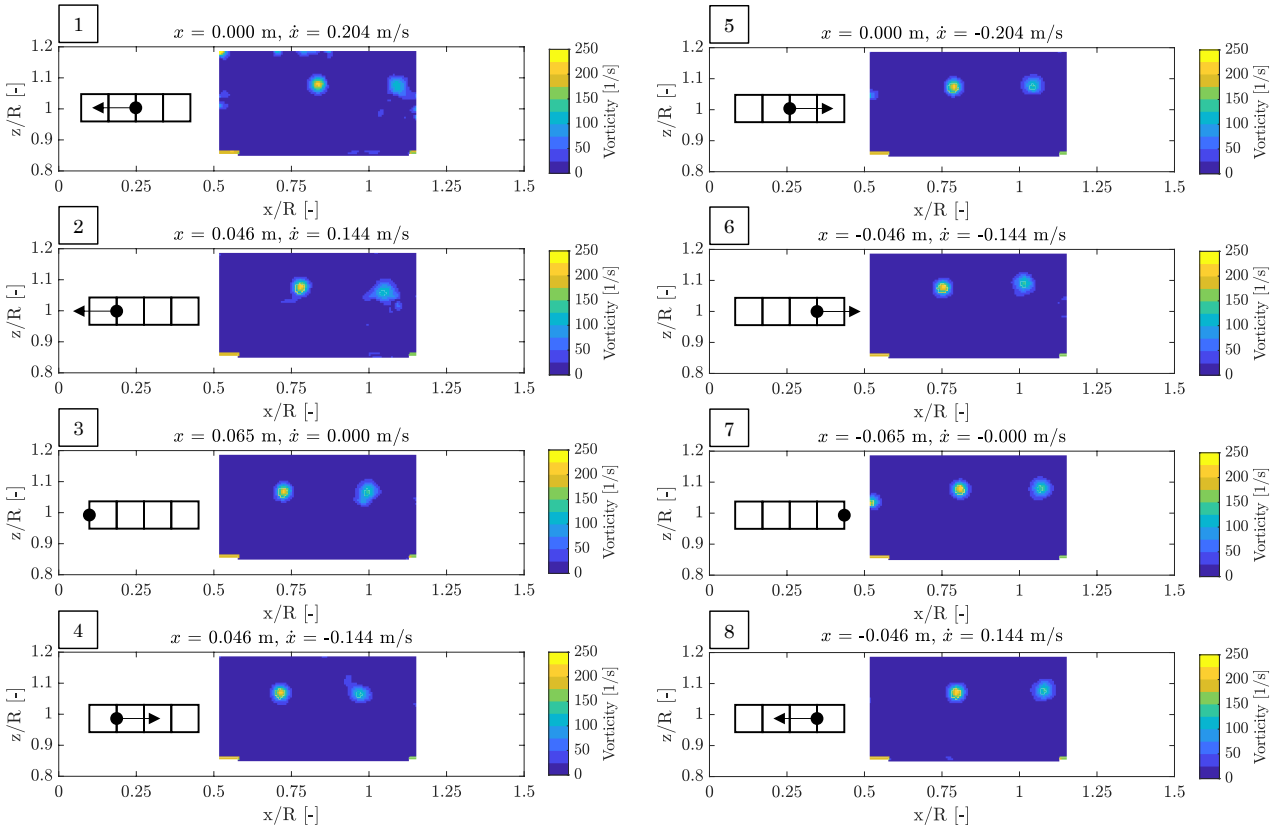

Figure 15. Vorticity for eight subsequent wind turbine positions in a surge cycle of frequency 0.5 Hz~~and~~ , amplitude 0.065 m, and RATED2 conditions. The blade-1 azimuth is always zero degrees. x/R and z/R are the axial and vertical distance from rotor rotor apex normalized by rotor radius. The origin of the axes is coincident with the rotor apex when the wind turbine is in the zero-surge position (see the Results ref. frame of Fig. 6).

is subjected to harmonic surge motion of several amplitudes and frequencies, selected to produce AoA variations confined in the linear lift-range. Thrust force measurements are carried out to study the full-turbine unsteady response. Measurements are compared to predictions of a quasi-steady rotor-disk model in order to assess the presence of unsteady effects. It is found that experimental data are aligned to quasi-steady theory ~~with good agreement~~ predictions up to a reduced frequency of 0.5. Above this frequency, unsteady effects may be present. However, ~~it is difficult to quantify the unsteady component of the thrust force by means of experiments. Its measurement is uncertain as it represents just a small fraction of the total rotor force.~~

~~Hub-height hot-wire anemometry and PIV surveys were~~ a thorough assessment of the experimental uncertainty, in particular the fraction related to the flexible response of the turbine tower, needs to be carried out to ~~investigate how the wake of~~ confirm the unsteady aerodynamic response for higher surge-motion frequencies. Near-wake measurements were performed with hot-wire probes to assess the effect of surge motion on the wind turbine ~~is affected by the surge motion. Hot-wire measurements~~

~~show that the mean~~ wake. The average hub-height velocity deficit with surge motion is the same as ~~with still wind turbine. On the other side, the spectral content of the wake clearly shows the trace of the imposed surge motion. In particular, the surge motion adds energy to the wake, and the energy increment~~ for still turbine. The wake spectral content is increased in correspondence of the surge-motion frequency: the increment (up to 9% compared to the steady case) is proportional to the maximum surge velocity. ~~PIV measurements, which are~~ A spatial analysis suggests that the largest increment is in the outer region of the rotor in RATED conditions, and in correspondence of the most loaded sections of the blade in the ABOVE condition. PIV measurements phase-locked to the ~~wind~~ turbine position in the surge cycle and to the rotor azimuth, show that ~~the~~ surge motion modifies the travel speed of the blade-tip vortex, that varies periodically ~~at the frequency of the surge motion~~with the surge-motion frequency.

The experiment ~~highlighted~~ posed some research questions that are still ~~opened~~ open and could be answered with further ~~investigations. In detail~~investigation:

- the coupled ~~dynamics of~~ rotor and platform rigid-body ~~motions~~ response is crucial for ~~the~~ control of floating wind turbines. Because of this ~~coupled dynamics~~coupling, closed-loop pitch-to-feather control strategies may lead to an unstable response of the system ~~Larsen and Hanson (2007); Jonkman (2008); van der Veen et al. (2012)~~(see for example the work of Larsen and Hanson (2007); Jonkman (2008); van der Veen et al. (2012)). One plausible solution is to design the controller based on a reduced-order model of the FOWT ~~Lemmer (ne Sandner)~~(Lemmer (ne Sandner)). In state-of-the-art control-design models, ~~the rotor aerodynamics is~~ rotor-integral aerodynamic forces are often introduced by means of quasi-steady theory ~~Fontanella et al. (2020); Lemmer et al. (2020)~~(Fontanella et al. (2020); Lemmer et al. (2020)). In order to improve the current control ~~practice~~methodologies, it would be useful to develop a control-oriented model of the unsteady thrust force. Experimental data ~~would be useful~~ are needed to calibrate and validate such a model~~.~~;

- the platform pitch mode ~~is very sensitive to the interaction with rotor~~ response is tightly coupled with rotor response, and a correct description of this phenomenon is essential in model-based wind turbine control strategies. Moreover, numerical simulations like those of Wise and Bachynski (2020) have shown that pitch motion has a strong influence on ~~the~~ vertical wake deflection~~Wise and Bachynski (2020), which~~ , and this phenomenon has the potential to be exploited for farm control purposes ~~. The pitch shares some similarities with the surge mode, as it causes~~ (Nanos et al. (2020)). Surge and pitch motion are similar as both cause an along-wind motion of the rotor. However, in the surge case, the ~~wind speed variation~~ variation of wind speed across the rotor is uniform, whereas in the pitch case, the flow seen by the rotor is skewed. ~~It may be worth carrying out experiments for the~~ Future wind-tunnel experiments should focus on platform pitch motion;

- unsteady aerodynamic effects appear to be more relevant ~~at the higher reduced frequencies~~for increased reduced-frequency of surge-motion. It would be ~~interesting to investigate surge-frequencies~~ worth investigating surge-motion frequencies higher than those considered in this experiment. This ~~is in general complex because of the risk of exciting the flexible modes of the wind turbine scale model. A potential solution is represented by numerical experiments. Numerical models~~

~~could~~ can be complicated by the flexible response of the turbine model. The turbine fore-aft mode is set by tower stiffness and weight of the rotor-nacelle assembly. Frequency is increased by reducing the latter and increasing the former. Slight stiffness increments are possible modifying the tower design, whereas RNA mass is heavily constrained by the mass of actuators (generator and pitch), control electronics, and sensors, that are commercial components, and cannot be modified. Numerical models can support experiments and circumvent the limitations of the latter. Numerical tools may be validated based on the experimental data ~~that are~~ already available, and then used to study ~~the other conditions , which~~ those conditions that may be unpractical to explore with experiments;

- ~~the interaction between surge motion and wind turbine wake deserves further attention. A better understanding of the wake inflow may help explaining the unsteady behavior of the rotor thrust force. Moreover, it would lead to improved engineering wake models, which are needed for the design and optimization of future floating wind farms.~~ quantifying uncertainty of the experiment results is important to interpret them correctly. The UNAFLOW dataset is currently utilized in the OC6 project, and one of the project key goals is to quantify uncertainty of data used for codes validation. A test campaign like the one discussed in this paper but dedicated to uncertainty quantification is currently planned. Uncertainty could be assessed with a methodology similar to that used by Robertson et al. (2020) for wave-basin tests.

Data availability. The dataset of the UNAFLOW experiment is accessible at `https://doi.org/10.5281/zenodo.4740005`.

Appendix A: Test matrices

Table A1. RATED1 test matrix (RS is the rotor speed, β is the rotor collective pitch angle). The CW, AW, PIV columns indicates wether if a cross-wind, along-wind or PIV measurement of the wake was carried out.

V [m/s]	f_s [Hz]	A_s [m]	V_w^* [-]	TSR [-]	RS [rpm]	β [deg]	CW	AW	PIV
2.5	0.125	0.125	8.62	7.5	150	0			
2.5	0.125	0.120	8.62	7.5	150	0			
2.5	0.125	0.080	8.62	7.5	150	0			
2.5	0.125	0.040	8.62	7.5	150	0			
2.5	0.250	0.080	4.31	7.5	150	0			
2.5	0.250	0.060	4.31	7.5	150	0			
2.5	0.250	0.040	4.31	7.5	150	0			
2.5	0.250	0.020	4.31	7.5	150	0			
2.5	0.500	0.040	2.16	7.5	150	0			
2.5	0.500	0.030	2.16	7.5	150	0			
2.5	0.500	0.020	2.16	7.5	150	0			
2.5	0.500	0.010	2.16	7.5	150	0			
2.5	0.750	0.030	1.44	7.5	150	0			
2.5	0.750	0.020	1.44	7.5	150	0			
2.5	0.750	0.015	1.44	7.5	150	0			
2.5	0.750	0.007	1.44	7.5	150	0			
2.5	1.000	0.030	1.08	7.5	150	0			
2.5	1.000	0.025	1.08	7.5	150	0			
2.5	1.000	0.015	1.08	7.5	150	0			
2.5	1.000	0.008	1.08	7.5	150	0			
2.5	1.500	0.015	0.72	7.5	150	0			
2.5	1.500	0.010	0.72	7.5	150	0			
2.5	1.500	0.007	0.72	7.5	150	0			
2.5	1.500	0.0035	0.72	7.5	150	0			
2.5	2.000	0.010	0.54	7.5	150	0			
2.5	2.000	0.007	0.54	7.5	150	0			
2.5	2.000	0.005	0.54	7.5	150	0			
2.5	2.000	0.0025	0.54	7.5	150	0			

Table A2. RATED2 test matrix (RS is the rotor speed, β is the rotor collective pitch angle). The CW, AW, PIV columns indicates wether if a cross-wind, along-wind or PIV measurement of the wake was carried out.

V [m/s]	f_s [Hz]	A_s [m]	V_w^* [-]	TSR [-]	RS [rpm]	β [deg]	CW	AW	PIV
4.0	0.125	0.125	13.79	7.5	241	0	×	×	×
4.0	0.125	0.100	13.79	7.5	241	0			
4.0	0.125	0.065	13.79	7.5	241	0			
4.0	0.125	0.030	13.79	7.5	241	0	×		×
4.0	0.250	0.125	6.90	7.5	241	0			
4.0	0.250	0.100	6.90	7.5	241	0			
4.0	0.250	0.065	6.90	7.5	241	0			
4.0	0.250	0.030	6.90	7.5	241	0			
4.0	0.500	0.065	3.45	7.5	241	0	×	×	×
4.0	0.500	0.050	3.45	7.5	241	0			
4.0	0.500	0.035	3.45	7.5	241	0			
4.0	0.500	0.015	3.45	7.5	241	0	×		×
4.0	0.750	0.040	2.30	7.5	241	0			
4.0	0.750	0.030	2.30	7.5	241	0			
4.0	0.750	0.020	1.44	7.5	241	0			
4.0	0.750	0.010	1.44	7.5	241	0			
4.0	1.000	0.050	1.72	7.5	241	0			
4.0	1.000	0.035	1.72	7.5	241	0	×	×	×
4.0	1.000	0.025	1.72	7.5	241	0			
4.0	1.000	0.010	1.72	7.5	241	0	×		×
4.0	1.500	0.020	1.15	7.5	241	0			
4.0	1.500	0.015	1.15	7.5	241	0			
4.0	1.500	0.010	1.15	7.5	241	0			
4.0	1.500	0.005	1.15	7.5	241	0			
4.0	2.000	0.015	0.86	7.5	241	0			
4.0	2.000	0.0125	0.86	7.5	241	0			
4.0	2.000	0.008	0.86	7.5	241	0	×	×	×
4.0	2.000	0.004	0.86	7.5	241	0	×		×

Table A3. ABOVE test matrix (RS is the rotor speed, β is the rotor collective pitch angle). The CW, AW, PIV columns indicates wether if a cross-wind, along-wind or PIV measurement of the wake was carried out.

V [m/s]	f_s [Hz]	A_s [m]	V_w^* [-]	TSR [-]	RS [rpm]	β [deg]	CW	AW	PIV
6.0	0.125	0.125	20.69	5.5	265	12.5			
6.0	0.125	0.100	20.69	5.5	265	12.5			
6.0	0.125	0.065	20.69	5.5	265	12.5			
6.0	0.125	0.030	20.69	5.5	265	12.5			
6.0	0.250	0.125	10.34	5.5	265	12.5			
6.0	0.250	0.100	10.34	5.5	265	12.5			
6.0	0.250	0.065	10.34	5.5	265	12.5			
6.0	0.250	0.030	10.34	5.5	265	12.5			
6.0	0.500	0.100	5.17	5.5	265	12.5			
6.0	0.500	0.075	5.17	5.5	265	12.5			
6.0	0.500	0.050	5.17	5.5	265	12.5			
6.0	0.500	0.025	5.17	5.5	265	12.5			
6.0	0.750	0.065	3.45	5.5	265	12.5			
6.0	0.750	0.050	3.45	5.5	265	12.5			
6.0	0.750	0.030	1.44	5.5	265	12.5			
6.0	0.750	0.015	1.44	5.5	265	12.5			
6.0	1.000	0.070	2.59	5.5	265	12.5			
6.0	1.000	0.050	2.59	5.5	265	12.5			
6.0	1.000	0.035	2.59	5.5	265	12.5			
6.0	1.000	0.018	2.59	5.5	265	12.5			
6.0	1.500	0.030	1.72	5.5	265	12.5			
6.0	1.500	0.025	1.72	5.5	265	12.5			
6.0	1.500	0.015	1.72	5.5	265	12.5			
6.0	1.500	0.008	1.72	5.5	265	12.5			
6.0	2.000	0.018	1.29	5.5	265	12.5	×		
6.0	2.000	0.0125	1.29	5.5	265	12.5	×		
6.0	2.000	0.006	1.29	5.5	265	12.5	×		

Author contributions. AF revised the experimental dataset helping to get the most recent results. IB was responsible of the full-turbine experiments and helped define the experimental methodology. RM carried out the 2D experiments and processed the respective data. MB and AZ supervised and promoted the research activity. Finally, AF prepared the manuscript of this article with contribution from all co-authors.

Competing interests. The authors declare that they have no conflict of interest.

Acknowledgements. The UNAFLOW research project has been funded by EU-EERA (European Energy Research Alliance)/IRPWIND Joint Experiment 2017.

References

Bak, C., Zahle, F., Bitsche, R., Taeseong, K., Yde, A., Henriksen, L. C., Hansen, M. H., Jose, J. P. A. A., Gaunaa, M., and Natarajan, A.: The DTU 10-MW Reference Wind Turbine, DTU Wind Energy Report, 2013.

Bayati, I., Belloli, M., Bernini, L., and Zasso, A.: Wind tunnel validation of AeroDyn within LIFES50+ project: imposed Surge and Pitch tests, Journal of Physics: Conference Series, 753, 092 001, https://doi.org/10.1088/1742-6596/753/9/092001, https://doi.org/10.1088/1742-6596/753/9/092001, 2016.

Bayati, I., Belloli, M., Bernini, L., Giberti, H., and Zasso, A.: Scale model technology for floating offshore wind turbines, IET Renewable Power Generation, 11, 1120–1126, https://doi.org/10.1049/iet-rpg.2016.0956, 2017.

Bayati, I., Belloli, M., Bernini, L., and Zasso, A.: A Formulation for the Unsteady Aerodynamics of Floating Wind Turbines, With Focus on the Global System Dynamics, vol. Volume 10: Ocean Renewable Energy of *International Conference on Offshore Mechanics and Arctic Engineering*, https://doi.org/10.1115/OMAE2017-61925, https://doi.org/10.1115/OMAE2017-61925, v010T09A055, 2017a.

Bayati, I., Belloli, M., Bernini, L., and Zasso, A.: Aerodynamic design methodology for wind tunnel tests of wind turbine rotors, Journal of Wind Engineering and Industrial Aerodynamics, 167, 217 – 227, https://doi.org/https://doi.org/10.1016/j.jweia.2017.05.004, http://www.sciencedirect.com/science/article/pii/S0167610517301368, 2017b.

Bayati, I., Belloli, M., Bernini, L., and Zasso, A.: Wind Tunnel Wake Measurements of Floating Offshore Wind Turbines, vol. 137, pp. 214–222, https://doi.org/10.1016/j.egypro.2017.10.375, https://www.scopus.com/inward/record.uri?eid=2-s2.0-85032015856&doi=10.1016%2fj.egypro.2017.10.375&partnerID=40&md5=aac148722a514dec153f833fee76b361, 2017c.

Bayati, I., Facchinetti, A., Fontanella, A., Giberti, H., and Belloli, M.: A wind tunnel/HIL setup for integrated tests of Floating Offshore Wind Turbines, Journal of Physics: Conference Series, 1037, 052 025, https://doi.org/10.1088/1742-6596/1037/5/052025, https://doi.org/10.1088%2F1742-6596%2F1037%2F5%2F052025, 2018.

Belloli, M., Bayati, I., Facchinetti, A., Fontanella, A., Giberti, H., La Mura, F., Taruffi, F., and Zasso, A.: A hybrid methodology for wind tunnel testing of floating offshore wind turbines, Ocean Engineering, 210, https://doi.org/10.1016/j.oceaneng.2020.107592, https://www.scopus.com/inward/record.uri?eid=2-s2.0-85085751799&doi=10.1016%2fj.oceaneng.2020.107592&partnerID=40&md5=e3b5533c595a58bc2d7e7684dc63bb95, 2020.

Bianchi, F., de Battista, H., and Mantz, R.: Wind Turbine Control Systems, Springer, https://doi.org/10.1007/1-84628-493-7, 2007.

Boorsma, K. and Caboni, M.: Numerical analysis and validation of unsteady aerodynamics for floating offshore wind turbines, TNO 2020 R11345, 880224, http://resolver.tudelft.nl/uuid:10b69f85-dd5a-4f74-ac68-fdc62c01ead3, 2020.

Bredmose, H., Lemmer, F., Borg, M., Pegalajar-Jurado, A., Mikkelsen, R., Larsen, T. S., Fjelstrup, T., Yu, W., Lomholt, A., Boehm, L., and Armendariz, J. A.: The Triple Spar campaign: Model tests of a 10MW floating wind turbine with waves, wind and pitch control, Energy Procedia, 137, 58 – 76, https://doi.org/https://doi.org/10.1016/j.egypro.2017.10.334, http://www.sciencedirect.com/science/article/pii/S1876610217352943, 14th Deep Sea Offshore Wind R&D Conference, EERA DeepWind'2017, 2017.

Chakraborty, P., Balachandar, S., and Adrian, R. J.: On the relationships between local vortex identification schemes, Journal of Fluid Mechanics, 535, 189–214, https://doi.org/10.1017/S0022112005004726, 2005.

Cormier, M., Caboni, M., Lutz, T., Boorsma, K., and Kramer, E.: Numerical analysis of unsteady aerodynamics of floating offshore wind turbines, Journal of Physics: Conference Series, 1037, 072 048, https://doi.org/10.1088/1742-6596/1037/7/072048, https://doi.org/10.1088%2F1742-6596%2F1037%2F7%2F072048, 2018.

de Vaal, J., Hansen, M., and Moan, T.: Effect of wind turbine surge motion on rotor thrust and induced velocity, Wind Energy, 17, 105–121, https://doi.org/https://doi.org/10.1002/we.1562, https://onlinelibrary.wiley.com/doi/abs/10.1002/we.1562, 2014.

Farrugia, R., Sant, T., and Micallef, D.: Investigating the aerodynamic performance of a model offshore floating wind turbine, Renewable Energy, 70, 24 – 30, https://doi.org/https://doi.org/10.1016/j.renene.2013.12.043, http://www.sciencedirect.com/science/article/pii/S0960148114000147, Special issue on aerodynamics of offshore wind energy systems and wakes, 2014.

Fontanella, A., Al, M., van der Hoek, D., Liu, Y., van Wingerden, J., and Belloli, M.: A control-oriented wave-excited linear model for offshore floating wind turbines, Journal of Physics: Conference Series, 1618, 022 038, https://doi.org/10.1088/1742-6596/1618/2/022038, https://doi.org/10.1088%2F1742-6596%2F1618%2F2%2F022038, 2020.

Fu, S., Jin, Y., Zheng, Y., and Chamorro, L. P.: Wake and power fluctuations of a model wind turbine subjected to pitch and roll oscillations, Applied Energy, 253, 113 605, https://doi.org/https://doi.org/10.1016/j.apenergy.2019.113605, http://www.sciencedirect.com/science/article/pii/S0306261919312796, 2019.

Goupee, A., Koo, B., Kimball, R., Lambrakos, K., and Dagher, H.: Experimental Comparison of Three Floating Wind Turbine Concepts, vol. 136, https://doi.org/10.1115/OMAE2012-83645, 2012.

Goupee, A., Fowler, M., Kimball, R., Helder, J., and Ridder, E. J.: Additional wind/wave basin testing of the DeepCwind semisubmersible with a performance-matched wind turbine, 33rd International Conference on Ocean, Offshore and Arctic Engineering (OMAE) - San Francisco, CA, USA, 9B, https://doi.org/10.1115/OMAE2014-24172, 2014.

Goupee, A., Kimball, R., and Dagher, H.: Experimental observations of active blade pitch and generator control influence on floating wind turbine response, Renewable Energy, 104, 9–19, https://doi.org/10.1016/j.renene.2016.11.062, https://www.scopus.com/inward/record.uri?eid=2-s2.0-85004140568&doi=10.1016%2fj.renene.2016.11.062&partnerID=40&md5=f58a2d3fcc9d9b9870f64cecf8dc5c0a, 2017.

GVPM: .

Hu, H., Khosravi, M. M., and Sarkar, P.: An Experimental Investigation on the Performance and the Wake Characteristics of a Wind Turbine Subjected to Surge Motion, https://doi.org/10.2514/6.2015-1207, https://arc.aiaa.org/doi/abs/10.2514/6.2015-1207, 2015.

Jonkman, J.: Influence of Control on the Pitch Damping of a Floating Wind Turbine, https://doi.org/10.2514/6.2008-1306, https://arc.aiaa.org/doi/abs/10.2514/6.2008-1306, 2008.

Kimball, R., Goupee, A. J., Fowler, M. J., de Ridder, E.-J., and Helder, J.: Wind/Wave Basin Verification of a Performance-Matched Scale-Model Wind Turbine on a Floating Offshore Wind Turbine Platform, vol. Volume 9B: Ocean Renewable Energy of *International Conference on Offshore Mechanics and Arctic Engineering*, https://doi.org/10.1115/OMAE2014-24166, https://doi.org/10.1115/OMAE2014-24166, 2014.

Larsen, T. and Hanson, T.: A method to avoid negative damped low frequent tower vibrations for a floating, pitch controlled wind turbine, vol. 75, https://doi.org/10.1088/1742-6596/75/1/012073, https://www.scopus.com/inward/record.uri?eid=2-s2.0-34548156706&doi=10.1088%2f1742-6596%2f75%2f1%2f012073&partnerID=40&md5=da0d731b888cd0eaf76d9406fbe321d6, 2007.

Lemmer, F., Yu, W., Luhmann, B., Schlipf, D., and Cheng, P. W.: Multibody modeling for concept-level floating offshore wind turbine design, Multibody System Dynamics, 49, 203 – 236, https://doi.org/10.1007/s11044-020-09729-x, https://doi.org/10.1007/s11044-020-09729-x, 2020.

Lemmer (ne Sandner), F., Yu, W., Schlipf, D., and Cheng, P. W.: Robust gain scheduling baseline controller for floating offshore wind turbines, Wind Energy, 23, 17–30, https://doi.org/10.1002/we.2408, https://onlinelibrary.wiley.com/doi/abs/10.1002/we.2408, 2020.

Mancini, S., Boorsma, K., Caboni, M., Cormier, M., Lutz, T., Schito, P., and Zasso, A.: Characterization of the unsteady aerodynamic response of a floating offshore wind turbine, https://doi.org/10.5194/wes-2020-94, 2020.

Martin, H. R., Kimball, R. W., Viselli, A. M., and Goupee, A. J.: Methodology for Wind/Wave Basin Testing of Floating Offshore Wind Turbines, Journal of Offshore Mechanics and Arctic Engineering, 136, https://doi.org/10.1115/1.4025030, 2014.

Moriarty, P. and Hansen, A.: AeroDyn Theory Manual, https://www.nrel.gov/docs/fy05osti/36881.pdf, 2005.

Nanos, E. M., Letizia, S., Clemente, D. J. B., Wang, C., Rotea, M., Iungo, V. I., and Bottasso, C. L.: Vertical wake deflection for offshore floating wind turbines by differential ballast control, Journal of Physics: Conference Series, 1618, 022 047, https://doi.org/10.1088/1742-6596/1618/2/022047, https://doi.org/10.1088/1742-6596/1618/2/022047, 2020.

Robertson, A., Bachynski, E. E., Gueydon, S., Wendt, F., and Schünemann, P.: Total experimental uncertainty in hydrodynamic testing of a semisubmersible wind turbine, considering numerical propagation of systematic uncertainty, Ocean Engineering, 195, 106 605, https://doi.org/https://doi.org/10.1016/j.oceaneng.2019.106605, https://www.sciencedirect.com/science/article/pii/S0029801819307309, 2020.

Sauder, T., Chabaud, V., Thys, M., Bachynski, E. E., and Sæther, L. O.: Real-Time Hybrid Model Testing of a Braceless Semi-Submersible Wind Turbine: Part I - The Hybrid Approach, vol. Volume 6: Ocean Space Utilization of *International Conference on Offshore Mechanics and Arctic Engineering*, https://doi.org/10.1115/OMAE2016-54435, https://doi.org/10.1115/OMAE2016-54435, v006T09A039, 2016.

Schliffke, B., Aubrun, S., and Conan, B.: Wind Tunnel Study of a "Floating" Wind Turbine's Wake in an Atmospheric Boundary Layer with Imposed Characteristic Surge Motion, Journal of Physics: Conference Series, 1618, 062 015, https://doi.org/10.1088/1742-6596/1618/6/062015, https://doi.org/10.1088%2F1742-6596%2F1618%2F6%2F062015, 2020.

van der Veen, G., Couchman, I., and Bowyer, R.: Control of floating wind turbines, in: 2012 American Control Conference (ACC), pp. 3148–3153, https://doi.org/10.1109/ACC.2012.6315120, 2012.

Vermeer, L., Sazrensen, J., and Crespo, A.: Wind turbine wake aerodynamics, Progress in Aerospace Sciences, 39, 467 – 510, https://doi.org/https://doi.org/10.1016/S0376-0421(03)00078-2, http://www.sciencedirect.com/science/article/pii/S0376042103000782, 2003.

Wise, A. S. and Bachynski, E. E.: Wake meandering effects on floating wind turbines, Wind Energy, 23, 1266–1285, https://doi.org/10.1002/we.2485, https://onlinelibrary.wiley.com/doi/abs/10.1002/we.2485, 2020.